Accepted Manuscript

Permian rifting and isolation of New Caledonia: Evidence from detrital zircon geochronology

Matthew Campbell, Uri Shaanan, Gideon Rosenbaum, Charlotte Allen, Dominique Cluzel, Pierre Maurizot

PII: S1342-937X(18)30112-6
DOI: doi:10.1016/j.gr.2018.04.004
Reference: GR 1963

To appear in:

Received date: 18 October 2017
Revised date: 2 April 2018
Accepted date: 4 April 2018

Please cite this article as: Matthew Campbell, Uri Shaanan, Gideon Rosenbaum, Charlotte Allen, Dominique Cluzel, Pierre Maurizot , Permian rifting and isolation of New Caledonia: Evidence from detrital zircon geochronology. The address for the corresponding author was captured as affiliation for all authors. Please check if appropriate. Gr(2018), doi:10.1016/j.gr.2018.04.004

Permian rifting and isolation of New Caledonia: Evidence from detrital zircon geochronology

Matthew Campbell[1], Uri Shaanan[1], Gideon Rosenbaum[1], Charlotte Allen[2] Dominique Cluzel[3] and Pierre Maurizot[4]

[1]School of Earth and Environmental Sciences, The University of Queensland, Brisbane, QLD 4072, Australia

[2]School of Earth, Environmental and Biological Sciences, Queensland University of Technology, Brisbane, QLD 4001, Australia

[3]Institut des Sciences Exactes et Appliquées, University of New Caledonia, BP R4, 98851, Noumea, New Caledonia

[4]Service Géologique de Nouvelle-Calédonie, BP 465, 98 845, Noumea, New Caledonia

ABSTRACT

The island of New Caledonia is the second largest rock exposure of the continent Zealandia. The New Caledonian basement rocks have been interpreted as representing a late Paleozoic to Mesozoic intra-oceanic arc system that was possibly correlative to contemporaneous terranes in eastern Australia and New Zealand. In order to understand tectonic relationships between the basement rocks of New Caledonia and other eastern Gondwanan terranes, we obtained >2200 new U-Pb ages of detrital zircon grains from New Caledonia. Our new results, combined with a synthesis of previously published geochronological data, show abundant pre-Mesozoic zircon ages, but an absence of Early Permian to Middle Triassic ages, which are characteristic of eastern Gondwana magmatism. The results thus suggest that the

detritus of the New Caledonian basement was derived from a local Paleozoic continental fragment that was rifted from the margin of Gondwana, most likely in the Early Permian. The results imply that dispersal of the Gondwanan margins started earlier than the Late Cretaceous opening of the Tasman and Coral seas, consistently with the Mesozoic endemism of both New Caledonia and New Zealand.

KEY WORDS: New Caledonia, Southwest Pacific, East Gondwana, detrital zircon, terrane analysis.

1. INTRODUCTION

Phanerozoic subduction along the Gondwanan margins produced one of the most extensive orogenic belts in the history of Earth (Terra Australis; Cawood, 2005). Along the margin of eastern Gondwana, subduction-related tectonostratigraphic units constitute the crustal basement of both eastern Australia (Tasmanides; Glen, 2005; Rosenbaum, 2018) and the continental basement of the southwest Pacific region (Fig. 1; Zealandia; Mortimer et al., 2017). The continuity of this plate margin has been disrupted by a number of major phases of deformation that culminated in the opening of the Tasman and Coral seas and the oceanward dispersal of continental fragments of Zealandia (Gaina et al., 1998; Sutherland et al., 2001; Crawford et al., 2003; Seton et al., 2012; Matthews et al., 2015).

The continental crustal basement of the southeast Pacific region is almost entirely submerged and/or covered by younger sedimentary rocks. The island of New Caledonia constitutes the second largest exposure (after New Zealand) of Gondwanan basement in the southwest Pacific region (Fig. 1). Nevertheless, the connectivity or isolation of New Caledonia relative to the rest of Gondwana, and the exact tectonic

setting of the New Caledonian basement terranes (i.e. the overall configuration of the paleo-subduction boundary), have remained relatively poorly constrained.

In this paper, we present new U-Pb detrital zircon geochronological data from the basement terranes of New Caledonia (Fig. 2; Téremba, Koh-Central and Boghen terranes). The results enable us to examine the provenance of each of the New Caledonian basement terranes and to discuss their spatio-temporal relationships with respect of each other and to the margins of eastern Gondwana.

2. GEOLOGICAL SETTING

Prior to the opening of the Tasman and Coral seas in the Late Cretaceous (~100 Ma), Zealandia, Australia and Antarctica were parts of eastern Gondwana (Cawood, 1984; Mortimer et al., 2017). Permian to Early Cretaceous supra-subduction units are recognized in eastern Australia (Glen, 2005) and New Zealand (Fig. 1; Mortimer et al., 2014; Milan et al., 2017; Mortimer et al., 2017), but the continuation and connectivity of these subduction units across the southwest Pacific remains uncertain.

Pre-Late Cretaceous rocks that have been recovered from the submerged parts of North Zealandia (Fig. 1) include: (1) Carboniferous granite dredged from the Challenger Plateau (Tulloch et al., 1991); (2) Permian plutonic rocks dredged from the Dampier Ridge (McDougall et al., 1994); (3) Early Triassic and Late Jurassic plutonic rocks from the West Norfolk Rise (Mortimer et al., 1998); (4) Devonian-Cretaceous plutonic and metasedimentary rocks from the Taranaki Basin (Mortimer et al., 1997); and (5) Late Triassic and Early Jurassic rocks from the central Lord Howe Rise (Mortimer et al., 2015). In general, the submerged basement rocks from North Zealandia show similar ages to rocks from the Median Batholith in New Zealand and

New England Orogen in eastern Australia (Fig. 1; Mortimer et al., 2008; 2015).

New Caledonia is positioned among a series of marginal basins and volcanic arcs (Fig. 1; Fairway Ridge, New Caledonia Basin, Norfolk Ridge, and Loyalty Ridge). Two major groups of terranes are distributed along the length of New Caledonia. The first group includes Late Carboniferous to Middle Jurassic Gondwanan crustal basement terranes (Fig. 2a; Cluzel et al., 2012). The second group unconformably overlies the basement terranes, and consists of Late Cretaceous (Formation à charbon) to Early Eocene sedimentary units and a peridotite nappe (Fig. 2a; Cluzel et al., 2010; Cluzel et al., 2011; Cluzel et al., 2012). The northernmost part of the island consists of a high-pressure metamorphic belt (Koumac, Diahot and Pouebo units) that was metamorphosed during the Eocene (Fig. 2a, Clarke et al., 1997; Spandler et al., 2005; Pirard and Spandler, 2017).

2.1 Basement terranes of New Caledonia

2.1.1 Téremba Terrane

The Téremba Terrane is exposed in the area between Baie de Saint-Vincent and Baie de Téremba, and is subdivided into two units (Figs. 2b, c). The lower part of the stratigraphy is the Late Permian to Middle Triassic Baie de Téremba Group, which has an estimated thickness of ~1570 meters (Fig. 2c, d, 3; Mara and Moindou formations; Campbell, 1984; Campbell and Grant-Mackie, 1984; Campbell et al., 1985). Volcanic rocks dominate the Téremba Group (40-60%), composed of rhyolite, dacite, andesite and minor basalt, as well as ignimbrite, welded tuff, volcanic breccia and pyroclastic rocks (Fig. 4a; Maurizot et al., *in press*). A vitric dacite from the Baie de Téremba (Fig. 3) was dated at 214.3±1.5 Ma using the K-Ar method (Paris, 1981, p. 30), but this age may be younger than the emplacement age due to a possible argon loss. U-Pb dating of magmatic zircon from an andesitic hypabyssal body in the Baie

de Téremba yielded a 240±3 Ma emplacement age (Fig. 2c, 3; Maurizot et al., *in press*). The remainder of the group consists of sedimentary rocks that are commonly rich in plant debris, including silicified or pyritized trunks and stems (Fig. 4b; Campbell et al., 1985). Bioclastic marine sedimentary rocks are locally rich in fragments of the typical prismatic shelled bivalve subfamily *Atomodesmatinae* (Fig. 4c, d; Campbell, 1984; Campbell et al., 1985).

The rocks of the Mara and Moindou formations are unconformably overlain by Late Triassic – Early Jurassic (Ouarai, Ouamoui, Leprédour, and Bouraké formations) and Middle Jurassic (Tani and Ilots Testard formations) rocks of the Baie de Saint Vincent Group, with a combined estimated thickness of ~1760 m (Fig. 2c; Campbell, 1984; Campbell et al., 1985). The Ouamoui and Ouarai formations are composed of very coarse, massive volcaniclastic conglomerate and medium- to fine-grained sandstone beds, respectively (Fig. 3, 4e, g; Campbell, 1984; Campbell et al., 1985). The Ouamoui Formation is unconformably overlain by the Leprédour Formation, a well-bedded sequence of fine- to medium-grained sandstone dominated by fossils of the *Monotis* shells (Fig. 3, 4e, f; Campbell and Grant-Mackie, 1984; Campbell et al., 1985). The overlying Bouraké Formation and the Tani Formation were deposited in the uppermost Triassic (Rhaetian) - Early Jurassic, and consist of volcaniclastic sandstone beds intercalated with conglomerate and debris flow deposits (Fig. 3; Campbell and Grant-Mackie, 1984; Campbell et al., 1985). The Middle Jurassic Ilot Testard Formation consists of medium to coarse marine volcaniclastic sandstone and conglomerate, rich in wood fragments (Fig. 3; Meister et al., 2010).

Rocks within the Baie de Téremba and Baie de Saint-Vincent groups have been suggested to be derived from a proximal, calk-alkaline, intra-oceanic island arc system in a shallow marine, fore-arc basin, depositional setting (Campbell, 1984;

Campbell et al., 1985; Meffre, 1991; Meffre, 1995; Cluzel et al., 2012). Biostratigraphic and paleontological investigations have drawn tentative correlations between the Téremba Terrane to that of both the Brook Street and Murihiku terranes in New Zealand (Fig. 1; Paris, 1981; Campbell, 1984; Campbell and Grant-Mackie, 1984; Campbell et al., 1985; Meffre, 1995). In addition, a tentative geochemical correlation has been suggested for basalts in the Brook Street and Téremba terranes (Spandler et al., 2005).

2.1.2 Koh-Central Terrane

The Koh-Central Terrane consists of an ophiolite suite (Koh Ophiolite), comprising gabbro, dolerite, rare plagiogranite, island-arc tholeiite and boninitic pillow basalt (Fig. 2c, d; Paris, 1981; Campbell, 1984; Meffre, 1991; Meffre, 1995). U-Pb SHRIMP ages of primary zircon grains from plagiogranite in the Koh Ophiolite yielded 302±7 Ma (n=14) and 290±5 Ma (n=14) crystallization ages (Fig. 2c; Aitchison et al., 1998), representing the oldest dated rocks on the island.

Overlying the abyssal argillite of the Koh Ophiolite is a thick deep-marine succession of shale, overlain by Middle Triassic to Early Cretaceous siltstone and volcaniclastic rocks (Fig. 2c, 4h, i; Paris, 1981; Campbell, 1984; Meffre, 1991; Meffre, 1995; Cluzel et al., 2010; Maurizot et al., *in press*). Based on its stratigraphic characteristics and sedimentary facies, the Koh-Central Terrane has been suggested to represent a more distal, deeper offshore part of the same fore-arc basin system of the Téremba Terrane (Cluzel et al., 2012).

2.1.3 Boghen Terrane

The Boghen Terrane (Fig. 2) is composed of schistose unfossiliferous, volcanic and sedimentary accretionary complex rocks (Fig. 4i; Cluzel and Meffre, 2002; Maurizot et al., *in press*). These rocks have been metamorphosed at lower-greenschist to blueschist-facies, with a westward increasing metamorphic grade (Cluzel et al., 2012). Three sandstone samples that have been dated using U-Pb geochronology show well-defined Early Cretaceous detrital zircon age populations (Cluzel and Meffre, 2002; Adams et al., 2009; Cluzel et al., 2010). Sedimentary rocks of the Boghen Terrane likely formed within a deep-sea fan derived from mixed terrigenous and volcanic arc sources, which most likely accumulated on an oceanic crust (Cluzel and Meffre, 2002). The schistose lithology and westward increase in metamorphic grade indicate that the sediments of the Boghen Terrane were likely part of a west-dipping subduction complex (Cluzel and Meffre, 2002; Cluzel et al., 2012).

3. APPROACH AND METHOLODOLGY

3.1 Sample preparation and analytical methods

Heavy mineral separation was done for twenty-four representative sedimentary samples from different stratigraphic levels from the Téremba, Koh-Central and Boghen terranes (Fig. 2b, 3, Table. 1). Samples were washed and dried in a 65 degrees oven, and stepwise crushed until all material sieved through a 425 μm mesh. Clay minerals were washed, and magnetic minerals were removed using a Frantz Magnetic Separator. The non-magnetic fraction was put in a tapped funnel with methylene iodide (MEI) heavy liquid to obtain heavy mineral separates. Zircon grains were handpicked using a binocular microscope, and mounted in non-reactive epoxy resin. The mounted grains were polished to expose their inner sections, and imaged using both transmitted light (Zeiss AxioImager M2M microscope) and scanning

electron microscope (Jeol JSM5410LV).

Isotopic compositions were obtained using Agilent 8800 Laser Ablation Inductively Coupled Plasma Mass Spectrometer (LA-ICP-MS) at the Queensland University of Technology. Data acquisition of 17 isotopes involved 25 seconds of background measurement followed by 30 seconds of sample ablation in a He/Ar atmosphere using a laser beam diameter of 30 μm. A firing rate of 7 Hz and sample fluence of about 0.6 mJ/cm^2 was used at the sample site from an ESI New Wave Excimer Laser system with Trueline cell. A total dwell time for the 17 isotopes was 0.4 second, so that an ablation produced about 70 individual analyses. The ^{206}Pb, ^{207}Pb, ^{208}Pb, ^{238}U and ^{232}Th masses necessary for dating were counted for half the analytical time (0.04 second per mass). Their ratios were calibrated against Temora-2 (416.78±0.33 Ma; Black et al., 2004) and monitored using the Plešovice zircon (337.13±0.37 Ma; Sláma et al., 2008) as a secondary standard. Beyond Pb, U and Th concentrations, elemental concentrations were determined from the following isotopes: ^{31}P, ^{49}Ti, ^{89}Y, ^{91}Zr, ^{139}La, ^{180}Ta, ^{140}Ce, ^{141}Pr, ^{146}Nd or ^{147}Sm, ^{153}Eu, ^{163}Dy, ^{175}Lu and ^{178}Hf. The NIST SRM 610 glass standard was used to calculate trace-element concentration using Si as an internal standard and assuming a stoichiometric concentration of 32.8 %wt SiO_2 in zircon.

Data were processed using Iolite software (Paton et al., 2011), and error correlation was done according to Ludwig (2003). Intervals were automatically selected and then visually edited to exclude, where possible, obvious inclusions based on P, Ti and La concentration patterns: P >1000 ppm, Ti >90 ppm or La >10 ppm. For grains younger than 950 Ma, concordance was taken when ^{206}Pb/^{238}U and ^{207}Pb/^{235}U ages are in agreement with propagated 2 sigma standard error uncertainty (Paton et al., 2010). For grains older than 950 Ma, ^{207}Pb/^{206}Pb are reported for the concordant

grains. The percent common Pb and common Pb corrected ages were calculated using the correction that assumes that $^{206}Pb/^{238}U$, $^{207}Pb/^{235}U$, $^{208}Pb/^{232}Th$ and $^{207}Pb/^{206}Pb$ should yield similar ages. Commonly, grains this old (>950 Ma) are discordant not because of common Pb, but due to Pb loss; therefore, correction for common Pb was not attempted. The 'selected' age for an analysis was decided as follows: for grains less than 950 Ma, if both the corrected and uncorrected $^{206}Pb/^{238}U$ ages were deemed concordant ($^{206}Pb/^{238}U$ and $^{206}Pb/^{235}U$ ages overlapped within given uncertainty), the one closest to concordia was selected, excluding grains with more than 2% of all ^{206}Pb calculated as common. Data were disregarded for plotting if they had unusually large trace element concentrations of P >1000 ppm, Ti >90 ppm or La >10 ppm, indicating the likely presence of inclusions.

Data were collected in 10 sessions on 10 days over the course of 9 months with a total of ~450 analyses of each of the standard materials (Plešovice, Temora-2 and NIST 610 glass). For an analytical session, $^{206}Pb/^{238}U$ ages for Plešovice ranged between 325.7±4.6 and 346.7±2.7 Ma, suggesting a systematic population accuracy of about ±10 Ma for this material relative to Temora-2 (ratios propagated to 150 Ma indicate a systematic population accuracy of 5 Ma). For full details on LA-ICP-MS data acquisition and analytical results see supplementary material.

3.2 Data handling

Geochronological constraints on the time of deposition were tested against the stratigraphic order and biostratigraphic constraints. Maximum depositional ages were calculated following the following different methods provided by Dickinson and Gehrels (2009): (a) youngest single grain age (YSA); (b) youngest graphical age peak (YPP) controlled by the ages of more than one grain; (c) mean age of the youngest two or more grains that overlap in age at 1σ (YC1σ), (d) mean age of the youngest

three or more grains that overlap in age at 2σ (YC2σ), and, (e) 'youngest detrital zircon age' generated by Isoplot 2008 (YDZ).

Detrital zircon data of samples from each terrane that consisted of overlapping constraints for the time of deposition were merged. Merging multiple samples is shown to address the naturally occurring internal variations in the proportions of age populations (e.g., Shaanan et al., 2018b), as well as providing a sufficient yield of zircon ages to permit terrane analysis. The characteristic age spectra and temporal variations within each of the different New Caledonian terranes were then examined through cumulative proportion curves and kernel density estimates (Vermeesch, 2012).

4. RESULTS

A total of 2267 new U-Pb concordant ages were obtained from 3314 analyses of 3240 detrital zircon grains from 18 sedimentary samples (Fig. 2b). Out of the 2267 new concordant ages, 162 were obtained for corresponding rims and cores. Detailed information on individual samples is provided in Table 1.

4.1 Maximum depositional age constraints

Constraints on the time of deposition of 18 samples from 7 Mesozoic formations are presented in Figure 5. With the exception of one sample (023_NC), the youngest single grain (YSG) of each sample consistently overlapped with the mean age of the youngest overlapping two (1σ) or three (2σ) ages (YC1σ and YC2σ; Table 2). For the purpose of this work, we use the YC1σ ages as the maximum depositional age constraint (Table. 2). As demonstrated by Dickinson and Grehels (2009), the determination of maximum depositional ages based on the multiple-grains methods

(YC1σ and YC2σ) is consistently compatible with inferred age of deposition. In contrast, the youngest graphical peak (YPP) method commonly results in an overly conservative maximum depositional age, whereas substantial analytical uncertainties surround the use of the youngest single grain (YSG) and youngest detrital zircon (YDZ) age methods due to (1) a lack of reproducibility, and (2) a model age for which direct analytical confirmation is lacking (Dickinson and Grehels, 2009).

4.2 **Detrital zircon age spectra and terrane analysis**

In order to better understand the provenance and inferred tectonic setting of the New Caledonia basement terranes, we synthesized a combined geochronological dataset (total of 548 ages) comprising our data and earlier published data (Cluzel and Meffre, 2002; Adams et al., 2009; Cluzel et al., 2010). The grouping (by inferred age of deposition) defines three sets of data: Group A, Late Triassic to Early Jurassic (237–175 Ma); Group B, Middle to Late Jurassic (175-145 Ma), and Group C, Early Cretaceous (145-100 Ma). We use this group terminology henceforth, and present the merged data of the groups from each terrane in Figures 6, 7 and 8.

4.2.1 Téremba Terrane

Group A in the Téremba Terrane (Fig. 6a, b) includes samples from the Ouarai Formation (045_NC and 048_NC), Ouamoui Formation (055_NC), Leprédour Formation (005_NC, 046_NC and 050_NC) and Bouraké Formation (061_NC, 023_NC), which all show maximum depositional age constraints between 217 to 199 Ma (Figs. 5, 6a, b). Group B in the Téremba Terrane is recognized in samples from the Tani Formation (059_NC) and Ilots Testard Formation (021_NC and 022_NC), which show maximum depositional ages between 168 to 151 Ma (Figs. 5, 6a, b).

Group C in the Terémba Terrane is recognized in samples 002_NC, 003_NC and 004_NC (Fig. 3, 6a, b), which show maximum depositional age constraints of 145 Ma (Fig. 5).

The most prominent detrital zircon component of Group A is Triassic (62.5%), with major peaks at c. 230 Ma and c. 215 Ma, and an additional minor age population peak at c. 550 Ma (Figs. 7, 8a). The combined age spectra of samples from Group B is characterized by dominant Jurassic (97.1%) peaks at c. 180 Ma and c. 185 Ma, and a significant decrease in Paleozoic (0.8%) and Proterozoic (0.4%) age components relative to Group A (Figs. 7, 8a). Group C samples are characterized by large proportions of Jurassic (46.2%) and Triassic (29.5%) ages, with major peaks at c. 215 Ma and c. 195 Ma, and minor Paleozoic (14.3%) and Proterozoic (9.8%) age populations (Figs. 7, 8a).

4.2.2 Koh-Central Terrane

Samples 009_NC, 013_NC, 015_NC, 060_NC, 062_NC (this study), and samples TRB23 and NCAL15 from Adams et al. (2009) belong to Group A for the Koh-Central Terrane, with maximum depositional age constraints between 229 to 179 Ma (Fig. 5, 6c, d). Group B in the Koh-Central Terrane has maximum depositional age constraints of 152–150 Ma (Fig. 6c, d; Adams et al., 2009). Group C is recognized in samples NCAL10 and PM118 (Adams et al., 2009), which have maximum depositional age constraints of 121 Ma and 103 Ma, respectively (Fig. 6c, d).

In contrast to the Téremba Terrane, the merged datasets of Groups A, B, and C from the Koh-Central Terrane show a diverse range of ages in the Late Triassic-Late Jurassic (Groups A and B). The combined, prominent components of Group A for the Koh-Central Terrane are Proterozoic (51.8%), with age population peaks observed at

c. 1110 Ma, c. 915 Ma and c. 825 Ma (Figs. 6, 8b). Additional age population peaks are observed at c. 235 Ma, c. 340 Ma, c. 415 Ma, c. 530 Ma, and c. 595 Ma (Fig. 7, 8b). Other ages are less abundant, with 2.5% Archean ages and 17.6% Mesozoic ages (Fig. 7). Higher proportions of Mesozoic (22.2%) and Proterozoic (48.4%) ages are recognized in the combined dataset for Group B, with peaks at c. 160 Ma, c. 575 Ma, c. 780 Ma and c. 965 Ma (Figs. 7, 8b). The combined Group C samples from the Koh-Central Terrane show a major change in detrital zircon ages, comprising a high proportion of Mesozoic (85.2%) and Proterozoic (12.2%) components and no Paleozoic or Archean ages (Fig. 7). Two major peaks are present at c. 110 Ma and c. 130 Ma (Figs. 7, 8b).

4.2.3 Boghen Terrane

Despite repeated attempts to generate detrital zircon data from the Boghen Terrane, yields from our samples were insufficient and generated separates that were under 30 µm. However, 121 detrital zircon ages from three samples from previous studies (Cluzel and Meffre, 2002; Adams et al., 2009; Cluzel et al., 2010) were incorporated in our dataset (Fig. 6e, f). Samples FTNA2 and NCAL32 show maximum depositional age constraints of 119 Ma and 137 Ma, respectively, whereas sample NCB154 yielded an earlier maximum depositional age constraint of 191 Ma.

Based on the scarce published ages above, it seems that age spectra of the Boghen Terrane are rather similar to those from the Koh-Central Terrane (Fig. 8b, c). The most prominent component of Group A is Proterozoic (76.6%) (Figs. 7, 8c). Other age components are Mesozoic (20%) and Paleozoic (3.3%) (Fig. 7, 8c). Data from Group C include 30 concordant ages, which provide a constraint for the timing of deposition but are deemed insufficient for terrane analysis (Figs. 7, 8c).

4.3 Rims and cores of detrital zircon

The majority of zircon grains with rims younger than 258 Ma are characterised by homogenous ages, whereby the core ages are similar to the rim ages (Fig. 8d, e). In 16 of the 69 doubly-analysed grains from 16 samples (Table. 1 and supplementary material), the cores are significantly older (Fig. 8d, e). There is no dominant cluster of core age populations for rims younger than 258 Ma, with ages of inherited cores variably ranging between ~330 Ma and ~1100 Ma (Fig 8d, e). For rims older than 258 Ma, most grains too are age-homogenous, with few cores that are distinctly older (Fig. 8d, e; 900 – 1300 Ma).

5. Discussion

5.1. Age of the New Caledonia basement

Geochronological results from the Koh-Central Terrane show that the youngest maximum depositional age constraints from five samples are 229-179 Ma (Fig. 5), thus indicating Late Triassic – Early Jurassic or younger deposition. Fauna observed in the Koh-Central Terrane include Ammonites of the genera *Hollandites* (Diener), *Leiophytlites* (Diener), *Prosphigites* (Mojsisivics), *Monotis* and *Inoceramus* fossils (Paris, 1981; Campbell et al., 1985; Meffre, 1991; Meffre, 1995), indicating a Middle Triassic (Anisian) to Jurassic age based on the New Zealand chronological chart (Raine et al., 2015), thus consistent with our results.

In contrast to the Koh-Central Terrane, age constraints from the Téremba Terrane, based on biostratigraphy and the New Zealand chronological chart (Raine et al., 2015), show inconsistencies with maximum depositional detrital zircon age constraints (Fig. 5). Samples from the Late Triassic (227.5 – 208.5 Ma) Ouarai (055_NC), Ouamoui (048_NC and 045_NC) and Leprédour Formation (005_NC, 046_NC and 050_NC) yielded maximum depositional age constraints that are

significantly younger than these of the associated fauna recorded of these formations (Fig. 5; Campbell and Grant-Mackie, 1984; Campbell et al., 1985; Meffre, 1995). Two samples from the Late Triassic- Early Jurassic (Otapirian – Aratauran; 208.5–188.9 Ma) Bouraké Formation (061_NC and 023_NC) yielded maximum depositional age constraints of 201.6±2.1 Ma and 214.3±3.9 Ma (n=4) (Fig. 5), with sample 023_NC being inconsistent with the suggested age of deposition.

Sample 059_NC from the Early Jurassic (Uronian; 188.9 – 176 Ma) Tani Formation yielded a maximum depositional age constraint of 167.0±5.3 Ma, which is inconsistent with biostratigraphic constraints (Fig. 5; Campbell and Grant-Mackie, 1984; Campbell et al., 1985). Two samples from the Middle Jurassic (Temalkan; 176 – 164.3 Ma) Ilots Testard Formation (021_NC and 022_NC) yeilded maximum depositional age constraints of 168.1±2.5 Ma (n=8) and 151.9±3.5 (n=4) (Fig. 5). Samples 002_NC, 003_NC and 004_NC were collected from the same coherent succession in the Téremba Terrane; thus the 145.6±3.4 Ma age from sample 003_NC is considered to represent the maximum depositional age, indicating a Late Jurassic-Early Cretaceous maximum age of deposition (Fig. 5). The maximum age constraints of samples 022_NC and 003_NC indicate that sedimentation in the Téremba Terrane did not end in the Middle Jurassic (Cluzel et al., 2012), but continued until the Late Jurassic-Early Cretaceous (Fig. 5).

Maximum age constraints based on detrital zircons in the Téremba Terrane either overlap or are somewhat younger (~10 Ma) than the fossil ages inferred from the New Zealand chronological chart (Fig. 5). This 10 Ma difference is based on several analyses that were taken in different sessions, indicating the discrepancy is beyond the systemic inaccuracies predicted by repeated analyses of Plešovice (~5 Ma). These inconsistencies could indicate that Mesozoic fauna in New Caledonia

evolved on an independent timeline in comparison to New Zealand, or that the Mesozoic biostratigraphic controls for the southwest Pacific (New Zealand included) require revisions.

5.2. Tectonic setting and provenance of New Caledonian basement

Group A, B and C for the Téremba Terrane and Groups C for the Koh-Central Terrane are dominated by a large portion of ages that closely approximate the time of deposition (Fig. 8a-c, 9), indicating syn-depositional volcanism, possibly in a fore-arc basin (Cawood et al., 2012). In contrast, Groups A and B for the Koh-Central Terrane and Groups A and C for the Boghen Terrane have older, more varied age ranges, indicating a different provenance (Fig. 8a-c, 9). A shift in the provenance is evident in the Koh-Central Terrane, in which connectivity with the source of the older grains (Groups A and B) was disrupted in the Cretaceous (Group C). The transition from older continental sources in Groups A and B to dominance of syn-depositional magmatism in Group C for the Koh-Central (Fig. 9) may indicate: (1) that the Koh-Central Terrane transitioned into a Cretaceous fore-arc position; or (2) that the source of the Gondwanan zircon of the Koh-Central Terrane was local, limited, and not exposed in the Cretaceous; or (3) New Caledonia became more isolated between ~130-100 Ma, associated with extension, and overwhelmed by rift-related siliceous volcanism leading up to and during the opening of the Tasman and Coral seas (e.g., Bryan et al., 2012; Barham et al., 2016).

The source of Late Triassic – Early Jurassic zircon age populations in the sedimentary rocks of the Téremba and Koh-Central terranes (Fig. 8a, b, c) is unclear. There are no igneous rocks of such ages in New Caledonia, but similar ages are known from the following subduction-related associations (Fig. 10a): (1) dredged granitic clasts from the Lord Howe Rise (Mortimer et al., 2015); (2) West Norfolk

Ridge (Mortimer et al., 1998); (3) Darran Suite in New Zealand (Mortimer et al., 1997; Muir et al., 1998; Mortimer et al., 2015); and (4) New England Orogen in eastern Australia (Li et al., 2012). Jurassic magmatic rocks are sparse in eastern Australia, except of abundant basalt and dolerite in Tasmania that unlikely contributed to the source of zircon (Fig. 10a). We suggest that the 180-150 Ma zircon age populations most likely represent a subduction-related zircon-producing source, which became inactive at around 150 Ma.

Early Permian to Middle Triassic magmatism is evident in the New England Orogen as well as in the Dampier Ridge (McDougall et al., 1994), and possibly West Norfolk Rise (Fig. 10a; Mortimer et al., 1998). Despite the extensive distribution of plutonic rocks of this age in eastern Australia, Early Permian to Middle Triassic zircon grains make up a very minor component of the basement strata of New Caledonia (Figs. 8a-c). The absence of these ages is specifically significant for the period 275-230 Ma, which in the New England Orogen, was associated with widespread magmatism (Fig. 10a; Shaw and Flood, 1981; Korsch et al., 2009a).

The ~415 and ~340 Ma age populations (Fig. 8b; Group A) and ~335 Ma age population (Fig. 8b; Group B) in the Koh-Central Terrane may correspond to magmatism in eastern Australia (Fig. 10a; Collins, 1996; Collins, 2002; Glen, 2005; Rosenbaum, 2018). Older age populations, and specifically the presence of 600-500 Ma, and 1300–900 Ma detrital zircon ages in the New Caledonian basement, suggest a contribution from reworked metasedimentary strata of the Tasmanides (Fergusson et al., 2017; Shaanan et al., 2018b). The occurrence of 16 older cores within zircon grains of Mesozoic rim ages also corresponds with the ages described above (335–1100 Ma; Fig. 8d, e). Oscillatory zoning and relatively low Th/U for these rims is consistent with magmatic zircon crystallization, implying that a sediment component

containing zircon grains was caught up in melting and magmatism, or that a sliver of continental basement was possibly re-melted in New Caledonia in the course of the Triassic-Jurassic magmatism.

5.3. Late Paleozoic to early Mesozoic tectonic evolution of New Caledonia

The deeper water sedimentary and underlying 'oceanic' crust of the Koh-Central Terrane implies that the terrane likely formed outboard of the shallow water and fossiliferous rocks of the Téremba Terrane (Groups A and B; Figs. 10b). The Boghen Terrane is situated farther east of the Téremba Terrane, roughly along strike with the Koh-Central Terrane, and has features of a subduction complex with broken formations and mafic/ultramafic mélanges (Fig. 10b; Cluzel et al., 2012). Thus, the eastward change from shallow marine (Téremba Terrane) to a deeper marine environment (Koh-Central Terrane), and an accretionary complex (Boghen Terrane), support previous suggestions for a westward dipping subduction system (Fig. 10b; Cluzel and Meffre, 2002; Cluzel et al., 2012).

Nd-Sr isotope values of $+0.9<\varepsilon_{Nd}<+3$ and $-0.4<\varepsilon_{Sr}<+25$ of Early Triassic to middle Cretaceous sandstones from the New Caledonia basement are indicative of magmatic source rocks derived from a juvenile mantle typical of island arc magmatism (Meffre, 1995; Adams et al., 2009). Magmatic rocks derived from juvenile mantle are also indicated by the composition of hafnium isotopes of Late Triassic/Jurassic (mean Hf = +6.5) and Early Cretaceous (mean Hf = +7.2) detrital zircon from the metamorphic units (Fig. 2a; Koumac, Diahot, Pouebo units) (Pirard and Spandler, 2017). Limited continental input was associated with this westward-dipping, subduction-related, island-arc magmatism in New Caledonia (Fig. 10b; Meffre, 1995; Cluzel and Meffre, 2002; Adams et al., 2009), but the presence of older, inherited Paleozoic zircon grains/cores indicates that magmatic recycling of a

potential sediment, or Gondwanan basement component occurred within this intra-oceanic arc system (Figs. 8d, e, 10b). The affinity of Nd-Sr isotopes with oceanic lithosphere (i.e., intra-oceanic arc magmatism) implies that the volume of the melted continental material was insufficient to modify the overall melt composition. The lack of inherited zircon grains in the Middle Triassic shallow level intrusive rocks of New Caledonia (Maurizot et al., *in press*) could suggest that a continental basement was located further outboard of New Caledonia, possibly in the Lord Howe Rise (Fig. 10a, b).

The Nd-Sr affinity of sedimentary rocks and Hf isotopes of detrital zircons, in combination with the Mesozoic intra-oceanic setting for New Caledonia contrasts with the previous suggestions that Gondwanan age populations were sourced from the continental interior (Adams et al., 2009). The higher abundance of Gondwanan aged zircon in the further ocean-ward, deep marine Koh-Central Terrane in respect to the Téremba Terrane (Fig. 8a-b), does not seem to agree with a direct continental drainage into the New Caledonian basement. Furthermore, the lack of Early Permian-Middle Triassic detrital zircon ages in all basement terranes in New Caledonia is inconsistent with a direct derivation from the continent interior. Thus, the presence of Gondwanan age material in the Mesozoic strata of New Caledonia (Fig. 8; Group A and B) requires an alternative explanation.

We propose that a thinned, Paleozoic continental fragment, which was rifted from the Gondwanan margins prior to the deposition of the late Paleozoic-Mesozoic Téremba, Koh-Central and Boghen terranes, was internally reworked and partly melted within the roots of a volcanic arc (Fig. 10b). This scenario is consistent with the evidence for an intra-oceanic arc environment (Nd-Sr and Hf isotope values), abundant occurrence of Gondwanan (Paleozoic-Proterozoic) ages in the deep marine

ocean-ward Koh-Central and Boghen terranes, and the absence of Early Permian to Middle Triassic age populations. The absence of the Early Permian to Middle Triassic ages implies that New Caledonia was separated and was distant from Gondwana in the Late Paleozoic, a conclusion consistent with the marked faunal and floral endemism that occurred during the Triassic – Jurassic (e.g. Paris, 1981; Cluzel et al., 2012). The existence of oceanic back-arc basins or marginal sediment traps most likely restricted late Paleozoic-Mesozoic detritus from east Australia reaching the New Caledonia basins.

Rifting of a thinned, Paleozoic continental fragment and development an intra-oceanic arc system most likely occurred during the Early Permian (300-280 Ma). During this period, eastern Gondwana was subjected to crustal extension, possibly in response to an eastward trench retreat (Korsch et al., 2009b; Shaanan et al., 2015). This period of Early Permian extension led to widespread formation of sedimentary basins, including the so-called East Australian Rift System and other smaller back-arc basins throughout eastern Australia (Fig. 10a; Korsch et al. 2009b; Campbell et al., 2015; Shaanan et al., 2015; Shaanan and Rosenbaum, 2018). This phase of rifting along the eastern Gondwana margin may explain the combination of an intra-oceanic setting for the New Caledonia basement rocks, the occurrence of Gondwana-derived zircon ages, and the absence of 275-230 Ma detritus. The implication for the tectonics of the southwest Pacific is that dispersal of continental fragments of eastern Gondwana may have occurred in the Early Permian, long before the Late Mesozoic opening of the Tasman and Coral seas.

6. Conclusion

New U-Pb zircon ages provide an insight into the tectonic setting and evolution of the late Paleozoic-Mesozoic basement terranes of New Caledonia. U-Pb geochronology data show that the Téremba Terrane has a distinct age spectra characteristic of a Mesozoic fore-arc basin, whereas the Koh-Central and Boghen terranes are characterized by diverse age spectra that also consist of significantly older age components. The absence of Early Permian to Middle Triassic detrital zircon ages in the New Caledonian basement terranes suggests isolation from eastern Gondwana during this time interval. The distribution of Paleozoic aged detritus within the basement terranes of New Caledonia implies a local (limited) source, possibly made of a thinned Paleozoic continental fragment that was rifted from the Gondwanan margins prior to the deposition of the late Paleozoic-Mesozoic Koh-Central, Téremba and Boghen terranes. We suggest that this rifted continental fragment was internally reworked and partly melted within the roots of an intra-oceanic arc, possibly beneath the Téremba Terrane and/or Lord Howe Rise, as evident in inherited zircon cores. The rifting of such a continental segment from the Gondwanan margins implies that dispersal of Gondwanan continental fragments within the southwest Pacific may have occurred before the Late Mesozoic, possibly in the course of a pronounced phase of extension in the Early Permian along the eastern Gondwanan margin.

7. Acknowledgements

The authors would like to thank Cassian Pirard for his helpful comments. We also thank Hamish Campbell, Chris Adams and staff at the Geological Survey of New Caledonia for assistance in the field and sample transportation. Karine Moromizato is thanked for technical support and guidance. This work was funded by a 2016 Geological Society of Australian Endowment Fund.

8. References

Adams, C.J., Cluzel, D., Griffin,W. L., 2009. Detrital-zircon ages and geochemistry of sedimentary rocks in basement Mesozoic terranes and their cover rocks in New Caledonia, and provenances at the Eastern Gondwanaland margin. Australian Journal of Earth Sciences 56, 1023–1047.

Aitchison, J.C., Ireland, T.R., Clarke, G.L., Cluzel, D., Davis, A. M., Meffre, S., 1998. Regional implications of U/Pb SHRIMP age constraints on the tectonic evolution of New Caledonia. Tectonophysic 299, 333–343.

Black, L.P., Kamo, S.L., Allen, C.M., Davis, D.W., Aleinikoff, J.N., Valley, J.W., Mundil, R., Campbell, I.H., Korsch, R.J., Williams, I.S., Foudoulis C., 2004. Improved $^{206}Pb/^{238}U$ microprobe geochronology by the monitoring of a trace-element-related matrix effect; SHRIMP, ID–TIMS, ELA–ICP–MS and oxygen isotope documentation for a series of zircon standards. Chemical Geology 205, 115–140.

Bryan, S.E., Cook, A.G., Allen, C.M., Siegal, C., Purdy, D.J., Greentree, J.S., Uysal, I.T., 2012. Early-mid Cretaceous tectonic evolution of eastern Gondwana: From silicic LIP magmatism to continental rupture. Episodes 35, 142–152.

Barham, M., Kirkland C.L., Reynolds, S., O'Leary, M. J., Evans, N.J., Allen H., Haines, P.W., Hocking, R.M., McDonald, B.J., Belousova, E., Goodall J., 2016. The answers are blowin' in the wind: Ultra-distal ashfall zircons, indicators of Cretaceous super-eruptions in eastern Gondwana, Geology,44, 643–646.

Campbell, H.J., 1984. Petrography and metamophism of the Téremba Group (Permian-Lower Triassic) and Baie de St. Vincent Group (Upper Triassic -

Lower Jurassic), New Caledonia. Journal of the Royal Society of New Zealand 14, 335–348.

Campbell, H.J., Grant-Mackie, J.A., 1984. Biostratigraphy of the Mesozoic Baie de St. Vincent Group, New Caledonia. Journal of the Royal Society of New Zealand 14, 349–366.

Campbell, H.J., Grant-Mackie, J.A., Paris, J.P., 1985. Geology of the Moindou-Téremba area, New Caledonia. Stratigraphy and structure of Téremba Group (Permian-Lower Triassic) and Baie de St.Vincent Group (Upper Triassic-Lower Jurassic). Geologie de la France 1, 19–36.

Campbell, M., Rosenbaum, G., Shaanan, U., Fielding, C.R., Allen, C., 2015. The tectonic significance of lower Permian successions in the Texas Orocline (Eastern Australia). Australian Journal of Earth Sciences 62, 789–806.

Cawood, P.A., 1984. The developement of the SW Pacific margin of Gondwana: correlations between the Rangitata and New England Orogens. Tectonics 3, 539–553.

Cawood, P.A., 2005. Terra Australis Orogen: Rodinia breakup and development of the Pacific and Iapetus margins of Gondwana during the Neoproterozoic and Paleozoic. Earth Science Reviews 69, 249–279.

Cawood, P.A., Hawkesworth, C.J., Dhuime, B., 2012. Detrital zircon record and tectonic setting. Geology 10, 875–878.

Clarke, G.L., Aitchison, J.C., Cluzel, D., 1997. Eclogites and Blueschists of the Pam Peninsula, NE New Caledonia: a Reappraisal. Journal of Petrology 38, 843–876.

Cluzel, D., Adams, C.J., Maurizot, P., Meffre, S., 2011. Detrital zircon records of Late Cretaceous syn-rift sedimentary sequences of New Caledonia: An Australian provenance questioned. Tectonophysics 501, 17–27.

Cluzel, D., Adams, C. J., Meffre, S., Campbell, H., Maurizot, P., 2010. Discovery of Early Cretaceous Rocks in New Caledonia: New Geochemical and U-Pb Zircon Age Constraints on the Transition from Subduction to Marginal Breakup in the Southwest Pacific. The Journal of Geology 118, 381–397.

Cluzel, D., Maurizot, P., Collot, J., Sevin, B., 2012. An outline of the Geology of New Caledonia; from Permian–Mesozoic Southeast Gondwanaland active margin to Cenozoic obduction and supergene evolution. Episodes 35, 72–86.

Cluzel, D. and Meffre, S., 2002. L'unité de la Boghen (Nouvelle-Calédonie, Pacifique sud-ouest): un complexe d'accrétion jurassique. Donneées radiochronologiques préliminaires U–Pb sur les zircons détritiques. Comptes Rendus Géosciences 334, 867–874.

Collins, W.J., 2002. Hot orogens, tectonic switching, and creation of continental crust. Geology 30, 535.

Collins, W.J., 1996. S- and I-type granitoids of the eastern Lachlan fold belt: products of three-component mixing. Transaction of the Royal Society of Edinburgh: Earth Sciences 88,171–179.

Crawford, A.J., Meffre, S., Symonds, P., 2003. Chapter 25 - 120 to 0 Ma tectonic evolution of the southwest Pacific and analogous geological evolution of the 600 to 220 Ma Tasman Fold Belt System. Geological Society of Australian Special Publication 22, 377–397.

Dickinson, W.R., Gehrels, G.E., 2009. Use of U–Pb ages of detrital zircons to infer maximum depositional ages of strata: A test against a Colorado Plateau Mesozoic database. Earth and Planetary Science Letters 288, 115–125.

Fergusson, C.L., Henderson, R.A., Offler, R., 2017. Chapter 13 - Late Neoproterozoic to early Mesozoic sedimentary rocks of the Tasmanides, Eastern Australia: Provenance switching associated with development of the East Gondwana active margin. In R. Mazumder (Ed.). Sediment provenance: Influences on compositional change from source to sink, 325–369.

Gaina, C., Müller, D.R., Royer, J.Y., Stock, J., Hardebeck, J., Symonds, P., 1998. The tectonic history of the Tasman Sea: A puzzle with 13 pieces. Journal of Geophysical Research: Solid Earth 103, 12413–12433.

Glen, R., 2005. The Tasmanides of Eastern Australia. Geological Society, London, Special Publications 246.

Korsch, R.J., Adams, C.J., Black, L.P., Foster, D.A., Fraser, G.L., Murray, C.G., Foudoulis, C., Griffin, W.L., 2009a. Geochronology and provenance of the Late Paleozoic accretionary wedge and Gympie Terrane, New England Orogen, eastern Australia. Australian Journal of Earth Sciences 56, 655–685.

Korsch, R.J., Totterdell, J.M., Cathro, D.L., Nicoll, M.G., 2009b. Early Permian East Australian Rift System. Australian Journal of Earth Sciences 56, 381–400.

Li, P.F., Rosenbaum, G., Rubatto, D., 2012. Triassic asymmetric subduction rollback in the southern New England Orogen (eastern Australia): the end of the Hunter-Bowen Orogeny. Australian Journal of Earth Sciences 59,. 965–981.

Ludwig, K.R., 2003. Users manual for ISOPLOT/EX, version 3. A geochronological toolkit for Microsoft Excel. Berkeley, Berkeley Geochronology Center Special Publication, 75.

Matthews, K.J., Williams, S.E., Whittaker, J.M., Müller, R.D., Seton, M., Clarke G.L., 2015. Geologic and kinematic constraints on Late Cretaceous to mid Eocene plate boundaries in the southwest Pacific. Earth Science Reviews 140, 72–107.

Maurizot, P., Cluzel, D., Meffre, S., Campbell, H., Collot, J., Sevin, B., in press. Pre-Late Cretaceous basement terranes of the Gondwana active margin. Memoir of the Geological Society of London Ed N. Mortimer Ch. 3.

McDougall, I., Maboko, M.A.H., Symonds, P.A., McCulloch, M.T., Williams, I.S., Kudrass, H.R., 1994. Dampier Ridge, Tasman Sea, as a stranded continental fragment. Australian Journal of Earth Sciences 41, 395–406.

Meffre, S., 1991. A Terrane Analysis of New Caledonia, with special reference to the Koh area. MSc (Hns) thesis, University of Sydney, Australia.

Meffre, S., 1995. Island arc-related ophiolites and sedimentary sequences in New Caledonia Australia. PhD Thesis, University of Sydney, Australia.

Meister, C., Maurizot, P., Grant-Mackie, J.A., 2010. Early Jurassic (Hettangian - Sinemurian) Ammonites from New Caledonia (French Overseas Territory, Western Pacific). Paleontological Research 14, 85–118.

Milan, L.A., Daczko, N.R., Clarke, G.L., 2017. Cordillera Zealandia: A Mesozoic arc flare-up on the palaeo–Pacific Gondwana Margin. Sci Rep 7, 261.

Mortimer, N., Campbell, H.J., Tulloch, A.J., King, P.R., Stagpoole, V.M., Wood, R.A., Rattenbury, M.S., Sutherland, R., Adams, C.J., Collot, J., Seton, M., 2017. Zealandia: Earth's Hidden Continent. GSA Today, 27–35.

Mortimer, N., Hauff, F., & Calvert, A.T., 2008. Continuation of the New England Orogen, Australia, beneath the Queensland Plateau and Lord Howe Rise. Australian Journal of Earth Sciences 55, 195–209.

Mortimer, N., Herzer, R.H., Gans, P.B., Parkinson, D.L., Seward, D., 1998. Basement geology from Three Kings Ridge to West Norfolk Ridge, Southwest Pacific Ocean; evidence from petrology, geochemistry and isotopic dating of dredge samples. Marine Geology 148, 135–162.

Mortimer, N., Rattenbury, M.S., King, P.R., Bland, K.J., Barrell, D.J.A., Bache, F., Begg, J.G., Campbell, H.J., Cox, S.C., Crampton, J.S., Edbrooke, S.W., Forsyth, P.J., Johnston, M.R., Jongens, R., Lee, J.M., Leonard, G.S., Raine, J.I., Skinner, D.N.B., Timm, C., Townsend, D.B., Tulloch, A.J., Turnbull, I.M., Turnbull, R.E., 2014. High-level stratigraphic scheme for New Zealand rocks. New Zealand Journal of Geology and Geophysics 57, 402–419.

Mortimer, N., Tulloch, A.J., Ireland, T.R., 1997. Basement geology of Taranaki and Wanganui Basins, New Zealand. New Zealand Journal of Geology and Geophysics 40, 223–236.

Mortimer, N., Turnbull, R.E., Palin, J.M., Tulloch, A.J., Rollet, N., Hashimoto, T., 2015. Triassic–Jurassic granites on the Lord Howe Rise, northern Zealandia. Australian Journal of Earth Sciences 62, 1–8.

Muir, R.J., Ireland, T.R., Weaver, S.D., Bradshaw, J.D., Evans, N.J., Eby, N., Shelley, D., 1998. Geochronology and geochemistry of a Mesozoic magmatic arc system, Fiordland, New Zealand. Journal of the Geological Society, London 155, 1037–1053.

Paris, J. P., 1981. Géologie de la Nouvelle–Calédonie. Un essai de synthèse, Bureau de Recherches Géologiques et Minières, Memoirs 113, 278.

Paton, C., Hellstrom, J., Paul, B., Woodhead, J., Hergt, J., 2011. Iolite: Freeware for the visualisation and processing of mass spectrometric data. Journal of Analytical Atomic Spectrometry 26, 2508.

Paton, C., Woodhead, J.D., Hellstrom, J.C., Hergt, J. M., Greig, A., Maas, R., 2010. Improved laser ablation U-Pb zircon geochronology through robust downhole fractionation correction. Geochemistry, Geophysics, Geosystems 11.

Pirard, C., Spandler, C., 2017. The zircon record of high–pressure metasedimentary rocks of New Caledonia: Implications for regional tectonics of the south–west Pacific. Gondwana Research. 46, 79–94.

Raine, J.I., Beu, A.G., Boyes, A.F., Campbell, H.J., Cooper, R.A., Cramption, J.S., Hollis, C.J., Morgans, H.E.G., 2015. Revised calibration of the New Zealand Geological timescale: NTZG2015/1. GNS Science Report.

Rosenbaum, G., 2018. The Tasmanides: Phanerozoic tectonic evolution of eastern Australia. Annual Review of Earth and Planetary Sciences 46, in press.

Seton, M., Müller, R.D., Zahirovic, S., Gaina, C., Torsvik, T., Shephard, G., Talsma, A., Gurnis, M., Turner, M., Maus, S., Chandler, M., 2012. Global continental and ocean basin reconstructions since 200Ma. Earth–Science Reviews 113, 212–270.

Shaanan, U., Rosenbaum, G., Hoy, D., Mortimer, N., 2018a. Late Paleozoic geology of Queensland Plateau (offshore northeastern Australia). Australian Journal of Earth Sciences, in press.

Shaanan, U., Rosenbaum, G., 2018. Detrital zircons as palaeodrainage indicators: Insights into southeastern Gondwana from Permian basins in eastern Australia. Basin Research 30, 36 – 47

Shaanan, U., Rosenbaum, G., Sihombing, F.M.H., 2018b. Continuation of the Ross–Delamerian Orogen: insights from eastern Australian detrital-zircon data. Australian Journal of Earth Sciences, 1–9.

Shaanan, U., Rosenbaum, G., Wormald, R., 2015. Provenance of the Early Permian Nambucca block (eastern Australia) and implications for the role of trench retreat in accretionary orogens. Geological Society of America Bulletin, p. B31178.1.

Shaw, S.E., Flood, R.H., 1981. The New England Batholith, eastern Australia: Geochemical variations in time and space. Journal of Geophysical Research: Solid Earth 86, 10530–10544.

Sláma, J., Košler, J., Condon, D.J., Crowley, J.L., Gerdes, A., Hanchar, J.M., Horstwood, M.S.A., Morris, G.A., Nasdala, L., Norberg, N., Schaltegger, U., Schoene, B., Tubrett, M.N., Whitehouse, M.J., 2008. Plešovice zircon — A new natural reference material for U–Pb and Hf isotopic microanalysis. Chemical Geology 249, 1–35.

Spandler, C., Rubatto, D., Hermann, J., 2005a. Late Cretaceous-Tertiary tectonics of the southwest Pacific: Insights from U-Pb sensitive, high-resolution ion microprobe (SHRIMP) dating of eclogite facies rocks from New Caledonia. Tectonics 24.

Spandler, C., Worden, K., Arculus, R., Eggins, S., 2005b. Igneous rocks of the Brook Street Terrane, New Zealand: implications from Permian tectonics of eastern Gondwana and magma genesis in modern intra-oceanic volcanic arcs. New Zealand Journal of Geology and Geophysics 48, 167–183.

Sutherland, R., King, P.R., Wood, R., 2001. Tectonic evolution of Cretaceous rift basins in South–Eastern Australia and New Zealand: implications for exploration risk assessment. In: Hill, K.C., Bernecker, T. (Eds.), Eastern Australasian Basins Symposium 2001. Petroleum Exploration Society of Australia Special Publication, 3–14.

Tulloch, A.J., Kimbrough, D.L., Wood, R.A., 1991. Carboniferous granite basement dredged from a site on the southwest margin of the Challenger Plateau, Tasman Sea. New Zealand Journal of Geology and Geophysics 34, 121–126.

Vermeesch, P., 2012. On the visualisation of detrital age distributions. Chemical Geology 321–313, 190–194.

FIGURE CAPTIONS

Figure 1: Bathymetric map of the southwest Pacific region showing major tectonic elements and domains.

Figure 2: Maps and sections of the study area. a. Tectonostratigraphic map of New Caledonia. b. Geological map of the New Caledonia basement terranes and sample localities (circles). c. Representative stratigraphic columns of the New Caledonia basement terranes. d. Schematic cross section (modified after Cluzel and Meffre, 2002) (cross section location shown on b).

Figure 3: Geological map, composite stratigraphic log and sampling localities from the Téremba Terrane. The stratigraphic log and corresponding fossil localities are after Meister et al. (2010).

Figure 4: Field photos from the Téremba Terrane (3 cm coin and 33 cm hammer shown for scale). a. Reworked, pyroclastic material with large, siltstone rip–up clasts. Mara Formation. (Coordinates: 21.81°S, 165.75°E). b. Well bedded, medium to coarse grained sandstone, siltstone and minor tuff exposure of the Mara Formation (Coordinates: 21.75°S, 165.70°E). c. Atomodesmatinae shell fossils. d. Atomodesmatinae shell fossil, Mara formation (Coordinates: 21.81°S, 165.75°E). e. Unconformable contact (red dashed line) between the Leprédour Formation and Ouamoui Formation (Coordinates: 22.03°S, 166.05°E). f. Monotis shells in the

Leprédour Formation (Sample 046_NC). g. Grain–supported conglomerate of the Ouamoui Formation (Sample 046_NC). h–i. Interbedded sandstone and siltstone turbidite sequences of the Koh–Central Terrane (coordinates: 21.71°S, 165.84°E and 21.69°S, 165.88°E, respectively). j. Foliated fine–grained sandstone/siltstones of the Boghen Terrane (coordinates: 20.98°S, 165.01°E).

Figure 5: Depositional age constraints for strata in the Téremba and Koh–Central terranes. Timescale after Raine et al. (2015).

Figure 6: Detrital zircon U/Pb age spectra of samples from the Téremba, Koh–Central and Boghen terranes. n = number of concordant/plotted analyses. Dashed lines indicate data from Adams et al. (2009), Cluzel et al. (2010) and Cluzel and Meffre (2002) (see Fig. 2b for sample locations). a. Cumulative proportion curves of samples from the Téremba Terrane. b. Kernel density estimates for samples from the Téremba Terrane. c. Cumulative proportion curves of samples from the Koh–Central Terrane. d. Kernel density estimates for samples from the Koh–Central Terrane. e. Cumulative proportion curves of individual samples from the Boghen Terrane. f. Kernel density estimates for samples from the Boghen Terrane.

Figure 7: Proportions of detrital zircon ages from a compiled U–Pb geochronology dataset for the Téremba, Koh–Central and Boghen terranes.

Figure 8: Detrital zircon age spectra of groups A, B and C within the three basement terranes. a. Kernel density estimates and cumulative proportion of combined samples from the Téremba Terrane. b. Kernel density estimates and cumulative proportion of samples from the Koh–Central Terrane. c. Kernel density estimates and cumulative proportion samples from the Boghen Terrane. d. U/Pb detrital zircon ages of corresponding rims and cores. e. Kernel density estimates (solid line) and relative probability (dashed line) plots of rims (red) and cores (blue).

Figure 9: Cumulative proportion curve for the time span between crystallization and inferred depositional ages (after Cawood et al. 2012), shown separately for Groups A, B and C within each basement terrane. Ages that proximate the time of deposition and only comprise a minor component of older ages are characteristic of fore–arc basins that typically drain magmatic arcs. In contrast, back–arc basins typically have an age spectra that reflects mix drainage of syn–depositional (arc) magmatism, and older (possibly continental interior) recycled sediments.

Figure 10: a. Tectonic map of the Southwest Pacific region, highlighting the occurrence of igneous rocks in eastern Australia, New Zealand and southwest Pacific Ocean (after Rosenbaum, 2018). Colored circles represent ages of igneous rocks in drill cores and dredge samples. West Norfolk Ridge (Mortimer et al., 1998); Lord Howe Rise (Mortimer et al., 2015); Dampier Ridge (McDougall et al., 1994); Queensland Plateau (Mortimer et al., 2008; Shaanan et al., 2018a). Abbreviations: DTO, Delamerian–Thomson Orogen; EARS, East Australian Rift System; LO, Lachlan Orogen; MO, Mossman Orogen; NEO, New England Orogen. b. Simplified schematic cross section of the basement terranes in New Caledonia illustrating the possible tectonic setting during the Late Triassic – Late Jurassic.

Table. 1: Sample list for U–Pb geochronology samples in New Caledonia.

Table. 2: Summary of maximum age constraints of samples from this study following methods by Dickinson and Gehrels (2009). n= Number of grains.

SUPPLEMENTARY DATA

1. ICP–MS analytical data

Table 1

Sample name	Latitude	Longitude	Terrane	Formation	Lithology	Mapped stratigraphic age	Concordant ages (n)/ total analyses (N)	Number of grains with concordant rim and cores (n)/Total number of grains (N)
023-NC	21°41'56.5"S	165°38'24.1"E	Téremba	Bouraké	Sandstone	Uronian, Middle Jurassic	180/141	3/5
061-NC	21°57'58.7"S	166°0'11.8"E	Téremba	Bouraké	Sandstone	Rhaetian, Late Triassic	66/42	3/9
009-NC	21°41'32.4"S	165°44'48.8"E	Koh-Central	Central	Sandstone	Ladinean, Middle Triassic	178/149	0/1
013-NC	21°33'43.8"S	165°50'21.9"E	Koh-Central	Central	Sandstone	Anisian, Middle Triassic	170/127	0/2
015-NC	21°9'24.3"S	165°25'20.7"E	Koh-Central	Central	Conglomerate	Norien, Late Triassic	62/29	1/3
060-NC	21°42'47.4"S	165°50'36.7"E	Koh-Central	Central	Sandstone	Norien, Late Triassic	167/112	7/14
062-NC	21°46'52.1"S	166°3'48.9"E	Koh-Central	Central	Sandstone	Carnian-Norian, Late Triassic	162/46	
005-NC	21°57'32.0"S	165°59'26.7"E	Téremba	Leprédour	Sandstone	Norien, Late Triassic	150/103	9/16
046-NC	22°1'57.7"S	166°3'1"E	Téremba	Leprédour	Sandstone	Norien, Late Triassic	169/100	5/15
050-NC	22°0'45.5"S	166°2'47.5"E	Téremba	Leprédour	Sandstone	Norien, Late Triassic	180/126	7/10
022-NC	21°42'21.9"S	165°34'48.7"E	Téremba	Ilots Testard	Sandstone	Bajocien-Bathonien, Middle Jurassic	200/94	0/0
021-NC	21°41'56.9"S	165°33'57.2"E	Téremba	Ilots Testard	Sandstone	Bajocien-Bathonien, Middle Jurassic	99/24	0/0
041-NC	21°44'52.7"S	165°42'0.3"E	Téremba	Mara	Sandstone	Permian		
054-NC	21°48'37.0"S	165°45'5.2"E	Téremba	Mara	Pyroclastic sandstone	Permian		
024-NC	21°44'52.4"S	165°42'0.3"E	Téremba	Mara	Sandstone	Permian		
032-NC	21°44'52.4"S	165°42'0.3"E	Téremba	Mara	Sandstone	Permian		
045-NC	22°1'53.8"S	166°3'10.0"E	Téremba	Ouaméoui	Conglomerate	Carnian-Norian, Late Triassic	32/22	4/9
048-NC	22°1'15.6"S	166°2'44.1"E	Téremba	Ouaméoui	Conglomerate	Carnian-Norien, Late Triassic	140/100	7/12
055-NC	21°44'6.2"S	165°42'53.2"E	Téremba	Ouarai	Conglomerate	Ladinian-Norien, Middle - Late triassic	160/95	2/7
011-NC	21°35'53.9"S	165°48'14.1"E	Boghen	Permian	Sandstone	Permian		
059-NC	21°42'34.7"S	165°36'50.1"E	Téremba	Tani	Sandstone	Uronian, Middle Jurassic	200/130	9/16
002-NC	22°11'38.5"S	166°26'42.4"E	Téremba	Undifferentiated	Sandstone	Late Triassic?	250/199	1/1
003-NC	22°11'38.5"S	166°26'42.4"E	Téremba	Undifferentiated	Conglomerate	Late Triassic?	500/431	19/22
004-NC	22°11'38.5"S	166°26'42.4"E	Téremba	Undifferentiated	Sandstone	Late Triassic?	249/197	4/7

Table 2

Maximal Depositional Constraints	YSG (1σ)	YPP	Yc1σ (n=+2)	YC2σ(3+)	YDZ		
					"1st Youngest"	"2nd Youngest'	"3rd Youngest"
023-NC	168.5±4.3 Ma	218 Ma	214.3±3.8 (n=4) (MSWD=0.62, probability = 0.60)	216.9±2.6 (n=9) (MSWD=0.67, probability =0.72)	169.17 + 11 - 13 Ma	185.62 + 7.4 - 10 Ma	194.38 + 8 - 8.7 Ma
061-NC	198.1±3.7 Ma	205 Ma	201.6±2.1 (n=11) (MSWD = 0.33, probability = 0.97)	204.3±1.5 (n=24) (MSWD = 0.87, probability = 0.64)	195 + 4.2 - 6.3 Ma	197 + 3.5 - 4.4 Ma	198.5 + 2.9 - 3.9 Ma
009-NC	217.2±3.5 Ma	231 Ma	228.0±2.3 Ma (n=13) (MSWD = 0.24, probability = 0.99)	228.9±2.0 Ma (n=16) (MSWD = 0.34, probability = 0.991)	217.1 + 5.2 - 8.3 Ma	220.3 + 4.8 - 6.1 Ma	222.8 + 3.6 - 5 Ma
013-NC	226.0±4.0 Ma	238 Ma	229.8±4.5 Ma (n=4) (MSWD = 0.48, probability = 0.69)	229.8±4.5 Ma (n=4) (MSWD = 0.48, probability = 0.69)	225.0 + 6.1-8.3	228.3 + 5.9 - 6.2 Ma	231.0 + 5.6 - 5.7 Ma
015-NC	177.0±5.8 Ma	180 Ma	179.5±2.0 Ma (n=11) (MSWD = 0.29, probability = 0.98)	180.1±1.9 Ma (n=13) (MSWD = 0.43, probability = 0.95)	165.0 + 7 - 7.8 Ma	173.7 + 3.7 - 6.2 Ma	175.0 + 3.7 - 4.1 Ma
060-NC	198.9±4.7 Ma	210 Ma	201.2±4.0 Ma (n=6) (MSWD = 0.20, probability = 0.96)	201.2±3.9 Ma (n=6) (MSWD = 0.20, probability = 0.96)	185.8 + 9 - 12 Ma	195.7 + 5.5 - 8.4 Ma	198.3 + 5.3 - 6.6 Ma
062-NC	221.1±5.1 Ma	245 Ma	226.4±5.3 Ma (n-3) (MSWD = 0.81, probability = 0.44)	226.4±5.2 Ma (n=3) (MSWD = 0.81, probability = 0.44)	199.37 + 9.1 - 9.6 Ma	220.8 + 8 - 11 Ma	227.0 + 6.8 - 8.3 Ma
005-NC	198.8±4.3 Ma	209 Ma	201.1±2.7 Ma (n=7) (MSWD = 0.28, probability = 0.95)	205.2±1.4 Ma (n=24) (MSWD = 0.79, probability = 0.75)	196.3 + 3.5 - 7.6 Ma	197.7 + 3.5 - 4.5 Ma	199.2 + 2.9 - 3.9 Ma
046-NC	201.9±4.7 Ma	209 Ma	205.5±2.5 Ma (n=13) (MSWD = 0.16, probability = 0.99)	207.3±3.6 Ma (n=24) (MSWD = 0.29, probability = 1.0)	197.7 + 4 - 8.2 Ma	199.7 + 3.2 - 5.6 Ma	200.6 + 3.2- 4.1 Ma
050-NC	195.4±3.9 Ma	204 Ma	199.2±2.9 Ma (n=8) (MSWD = 0.26, probability = 0.97)	201.9±1.7 Ma (n=24) (MSWD = 0.32, probability = 0.99)	193.3.8 + 3.8 - 7.2 Ma	195.0 + 3 - 5.2 Ma	196.0 + 2.8 - 4.1 Ma
022-NC	148.8±4.2 Ma	152 Ma	151.9±3.5 Ma (n=4) (MSWD = 0.43, probability = 0.73)	151.9±3.3 Ma (n=4) (MSWD = 0.43, probability = 0.73)	148.3 + 4.6 - 8.8 Ma	150.8 + 4.5 - 5.1 Ma	153.0 + 4.8 - 4.6 Ma
021-NC	163.7±4.4 Ma	172 Ma	168.1±2.5 Ma (n=8) (MSWD = 0.42, probability = 0.89)	169.1±2.2 Ma (n=10) (MSWD = 0.74, probability = 0.68)	163.0 + 3.8 - 8.9 Ma	165.0 + 3.4 - 5.1 Ma	166.3 + 3.2-4.1 Ma
045-NC	209.5±3.3 Ma	223 Ma	212.8±3.9 Ma (n=3) (MSWD = 0.82, probability = 0.44)	219.0±3.0Ma (n=6) (MSWD = 0.90, probability = 0.48)	199.6 + 6.9 - 6.8 Ma	212.9 + 4.9 - 7.3 Ma	215.7 + 4.3 - 5.6 Ma
048-NC	212.2±3.7 Ma	223 Ma	215.3±2.2 Ma (n=13) (MSWD = 0.26, probability = 0.99)	217.5±1.6 Ma (n=24) (MSWD = 0.53, probability = 0.97)	207.9 + 4.3 - 7.4 Ma	210.3 + 3.2 - 5.2 Ma	211.5 + 2.9 - 4.1 Ma
055-NC	212.0±4.2 Ma	224 Ma	216.3±2.6 Ma (n=6) (MSWD=0.32, probability = 0.90)	222.2±1.8 Ma (n=24) (MSWD=0.55, probability = 0.96)	205.6 + 6.2 - 10 Ma	209.0 + 4.9 - 7.6 Ma	211.3 + 4.1 - 6.5 Ma
059-NC	165.2±3.6 Ma	182 Ma	167.0±5.3 Ma (n=2) (MSWD = 0.61, probability = 0.43)	172.3±3.0 Ma (n=7) (MSWD = 0.90, probability = 0.54)	164.3 + 5.5 - 7.3 Ma	168.3 + 3.7 - 6 Ma	169.8 + 3.4 - 4.3 Ma
002-NC	178.1±3.0 Ma	202 Ma	179.2±2.9 Ma (n=4) (MSWD=0.13, probability = 0.94)	179.2±2.9 Ma (n=4) (MSWD=0.13, probability = 0.94)	150.4 + 6.5 - 5.5 Ma	163.7 + 6.1 - 6.5 Ma	176.3 + 4 - 5.5 Ma
003-NC	144.8±2.0 Ma		145.6±3.4 Ma (n=2) (MSWD = 0.14, probability = 0.71)	149.1±7.2 Ma (n=4) (MSWD = 3.2, probability = 0.022)	133.8 + 8.4 - 8.3 Ma	144.3 + 4.1 - 4.7 Ma	148.3 + 4.8 - 5.5 Ma
004-NC	165.3±2.4 Ma	195 Ma	166.9±3.6 Ma (n=2) (MSWD = 1.09, probability = 0.30)	169.8±6.4 Ma (n=4) (MSWD = 2.4, probability = 0.07)	165 + 4.6 - 5.2 Ma	168.8 + 4.5 - 4.6 Ma	171.8 + 4.3 - 4.3 Ma

Highlights

- Origin and tectonic evolution of basement terranes in New Caledonia revealed.
- Detrital zircons show absence of Early Permian to Middle Triassic ages.
- Paleozoic detritus suggest reworking and crustal melting of Gondwanan fragment
- Pre-late Mesozoic dispersal of Gondwanan fragments within the southwest Pacific
- Rifting was possibly associated with a pronounced phase of Early Permian extension

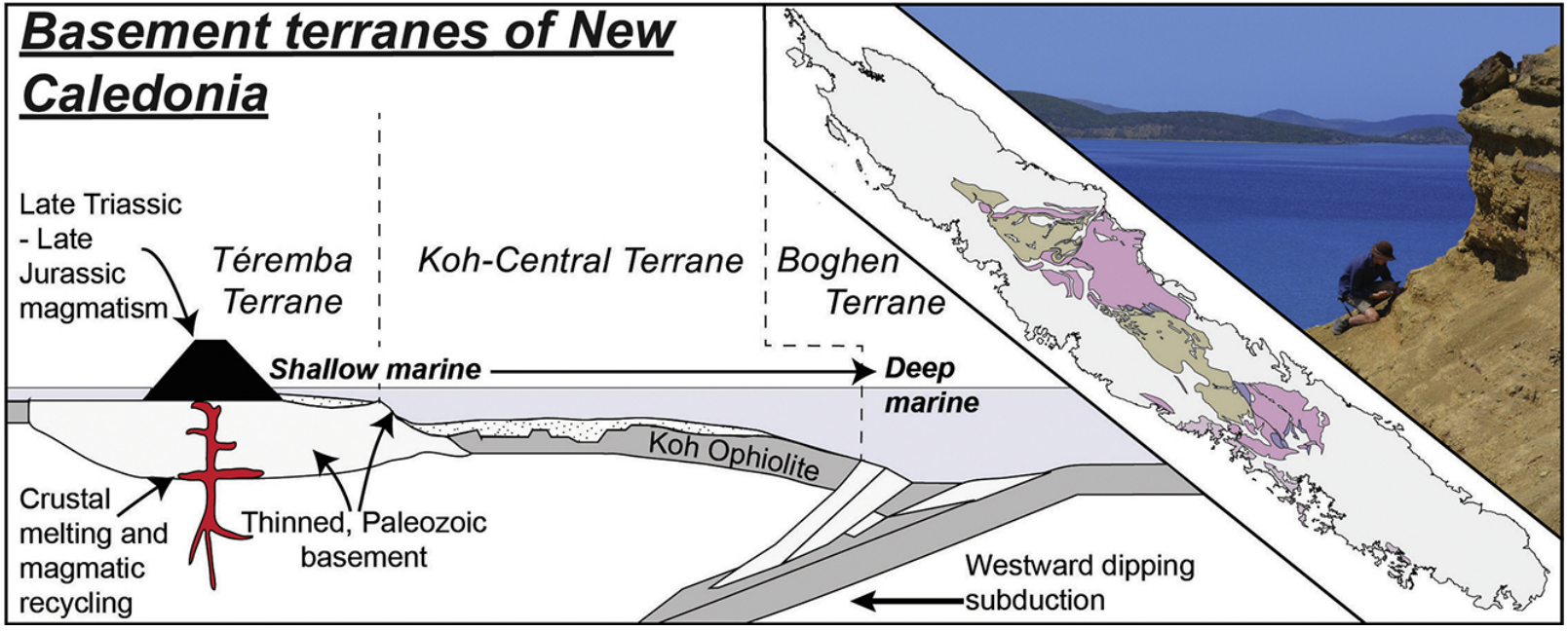

Graphics Abstract

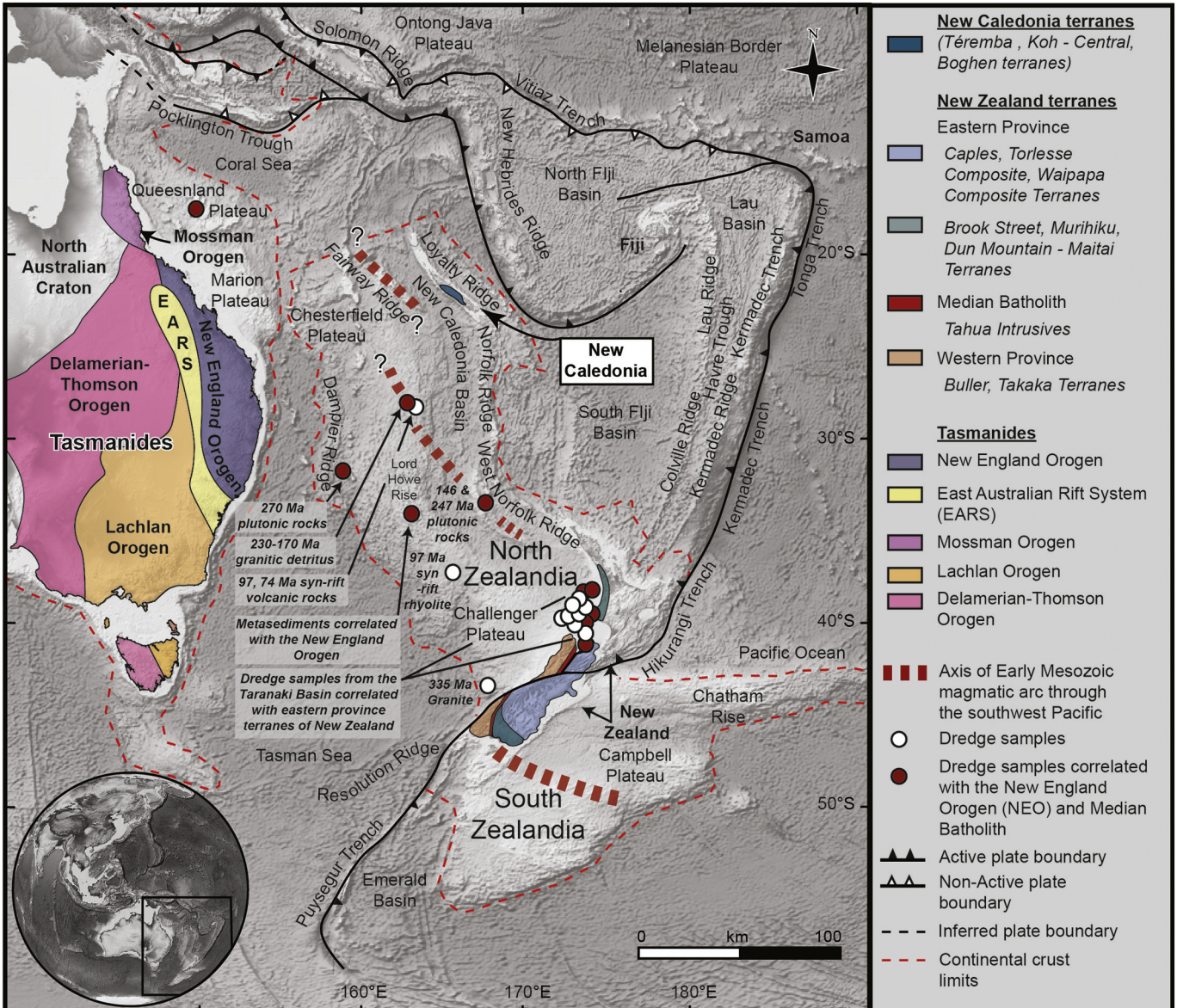
Ontong Java Plateau
Solomon Ridge
Melanesian Border Plateau
Vitiaz Trench
Pocklington Trough
Coral Sea
New Hebrides Ridge
North Fiji Basin
Samoa
Queensland Plateau
Lau Basin
Fiji
Tonga Trench
Mossman Orogen
North Australian Craton
Marion Plateau
Fairway Ridge
Loyalty Ridge
New Caledonia Basin
Chesterfield Plateau
New Caledonia
Lau Ridge
Havre Trough
Kermadec Ridge
Kermadec Trench
20°S
E A R S
New England Orogen
Delamerian-Thomson Orogen
Tasmanides
Dampier Ridge
Norfolk Ridge
West Norfolk Ridge
South Fiji Basin
Colville Ridge
Lord Howe Rise
30°S
270 Ma plutonic rocks
230-170 Ma granitic detritus
97, 74 Ma syn-rift volcanic rocks
146 & 247 Ma plutonic rocks
97 Ma syn-rift rhyolite
North Zealandia
Lachlan Orogen
Metasediments correlated with the New England Orogen
Challenger Plateau
40°S
Pacific Ocean
Hikurangi Trench
Dredge samples from the Taranaki Basin correlated with eastern province terranes of New Zealand
335 Ma Granite
Chatham Rise
New Zealand
Tasman Sea
Campbell Plateau
Resolution Ridge
South Zealandia
50°S
Puysegur Trench
Emerald Basin
0
km
100
160°E
170°E
180°E
N
New Caledonia terranes
(Téremba , Koh - Central, Boghen terranes)
New Zealand terranes
Eastern Province
Caples, Torlesse Composite, Waipapa Composite Terranes
Brook Street, Murihiku, Dun Mountain - Maitai Terranes
Median Batholith
Tahua Intrusives
Western Province
Buller, Takaka Terranes
Tasmanides
New England Orogen
East Australian Rift System (EARS)
Mossman Orogen
Lachlan Orogen
Delamerian-Thomson Orogen
Axis of Early Mesozoic magmatic arc through the southwest Pacific
Dredge samples
Dredge samples correlated with the New England Orogen (NEO) and Median Batholith
Active plate boundary
Non-Active plate boundary
Inferred plate boundary
Continental crust limits

Figure 1

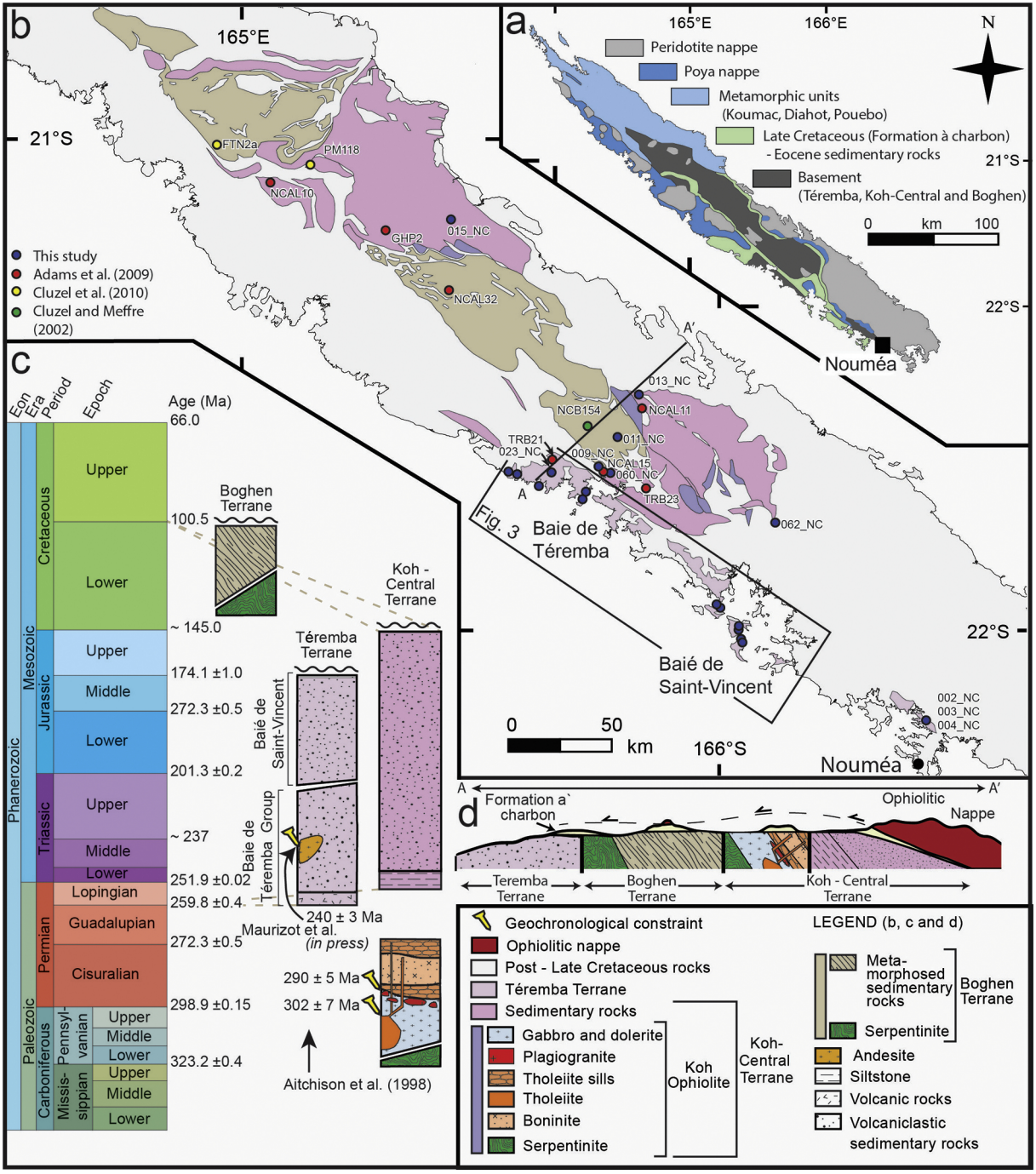
b
165°E
21°S
FTN2a
PM118
NCAL10
GHP2
015_NC
NCAL32
This study
Adams et al. (2009)
Cluzel et al. (2010)
Cluzel and Meffre (2002)
a
165°E
166°E
N
Peridotite nappe
Poya nappe
Metamorphic units
(Koumac, Diahot, Pouebo)
Late Cretaceous (Formation à charbon)
- Eocene sedimentary rocks
Basement
(Téremba, Koh-Central and Boghen)
0 km 100
21°S
22°S
Nouméa
A'
013_NC
NCAL11
NCB154
TRB21
023_NC
009_NC
011_NC
NCAL15
060_NC
TRB23
A
062_NC
Fig. 3
Baie de
Téremba
Baié de
Saint-Vincent
0 50 km
166°S
002_NC
003_NC
004_NC
Nouméa
c
Eon
Era
Period
Epoch
Age (Ma)
66.0
Phanerozoic
Mesozoic
Cretaceous
Upper
Lower
100.5
Boghen
Terrane
~ 145.0
Jurassic
Upper
Middle
Lower
174.1 ±1.0
272.3 ±0.5
201.3 ±0.2
Téremba
Terrane
Baié de
Saint-Vincent
Koh -
Central
Terrane
Triassic
Upper
Middle
Lower
~ 237
251.9 ±0.02
Baie de
Téremba
Group
Paleozoic
Permian
Lopingian
Guadalupian
Cisuralian
259.8 ±0.4
272.3 ±0.5
298.9 ±0.15
240 ± 3 Ma
Maurizot et al.
(in press)
290 ± 5 Ma
302 ± 7 Ma
Carboniferous
Pennsyl-
vanian
Upper
Middle
Lower
323.2 ±0.4
Missis-
sippian
Upper
Middle
Lower
Aitchison et al. (1998)
d
A
A'
Formation a`
charbon
Ophiolitic
Nappe
Teremba
Terrane
Boghen
Terrane
Koh - Central
Terrane
Geochronological constraint
Ophiolitic nappe
Post - Late Cretaceous rocks
Téremba Terrane
Sedimentary rocks
Gabbro and dolerite
Plagiogranite
Tholeiite sills
Tholeiite
Boninite
Serpentinite
Koh
Ophiolite
Koh-
Central
Terrane
LEGEND (b, c and d)
Meta-
morphosed
sedimentary
rocks
Boghen
Terrane
Serpentinite
Andesite
Siltstone
Volcanic rocks
Volcaniclastic
sedimentary rocks

Figure 2

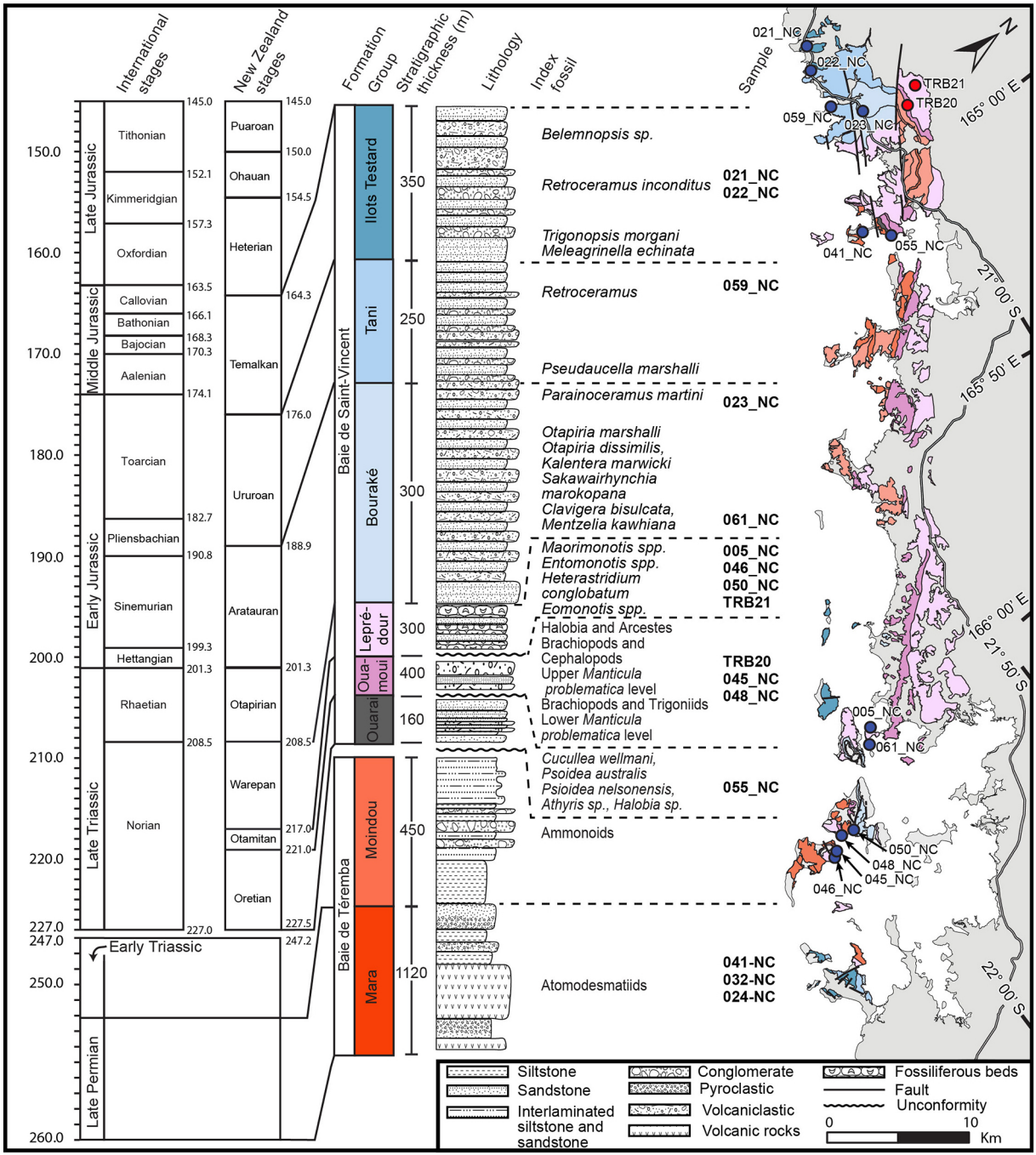
International stages
New Zealand stages
Formation
Group
Stratigraphic thickness (m)
Lithology
Index fossil
Sample
Late Jurassic
Middle Jurassic
Early Jurassic
Late Triassic
Late Permian
Tithonian
Kimmeridgian
Oxfordian
Callovian
Bathonian
Bajocian
Aalenian
Toarcian
Pliensbachian
Sinemurian
Hettangian
Rhaetian
Norian
Early Triassic
Puaroan
Ohauan
Heterian
Temalkan
Ururoan
Aratauran
Otapirian
Warepan
Otamitan
Oretian
Baie de Saint-Vincent
Baie de Téremba
Ilots Testard
Tani
Bouraké
Lepré-dour
Oua-moui
Ouarai
Moindou
Mara
350
250
300
300
400
160
450
1120
Belemnopsis sp.
Retroceramus inconditus
Trigonopsis morgani
Meleagrinella echinata
Retroceramus
Pseudaucella marshalli
Parainoceramus martini
Otapiria marshalli
Otapiria dissimilis,
Kalentera marwicki
Sakawairhynchia
marokopana
Clavigera bisulcata,
Mentzelia kawhiana
Maorimonotis spp.
Entomonotis spp.
Heterastridium
conglobatum
Eomonotis spp.
Halobia and Arcestes
Brachiopods and
Cephalopods
Upper Manticula
problematica level
Brachiopods and Trigoniids
Lower Manticula
problematica level
Cucullea wellmani,
Psoidea australis
Psioidea nelsonensis,
Athyris sp., Halobia sp.
Ammonoids
Atomodesmatiids
021_NC
022_NC
059_NC
023_NC
041_NC
055_NC
061_NC
005_NC
046_NC
050_NC
TRB21
TRB20
045_NC
048_NC
Siltstone
Sandstone
Interlaminated siltstone and sandstone
Conglomerate
Pyroclastic
Volcaniclastic
Volcanic rocks
Fossiliferous beds
Fault
Unconformity
0
10
Km

Figure 3

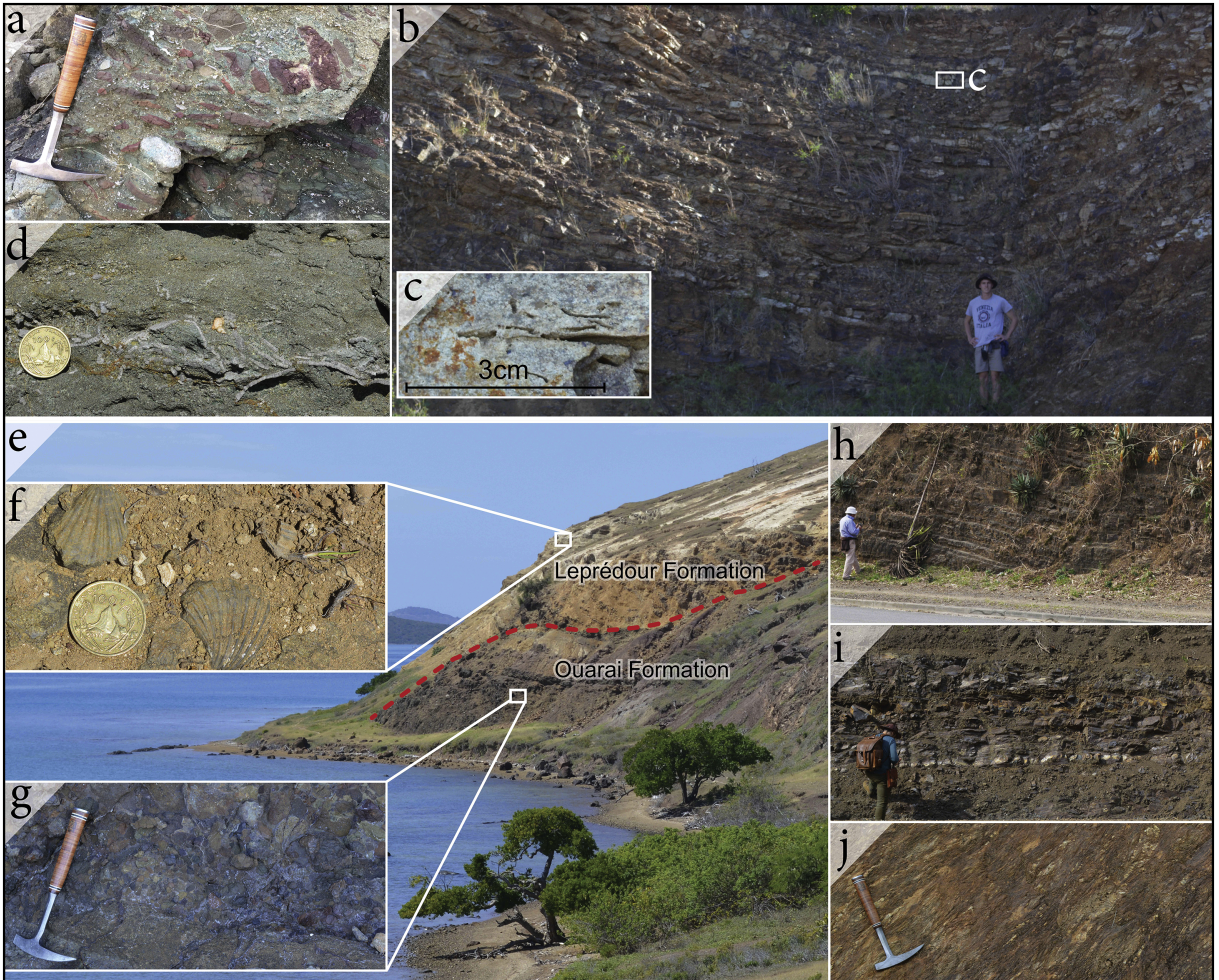

Figure 4

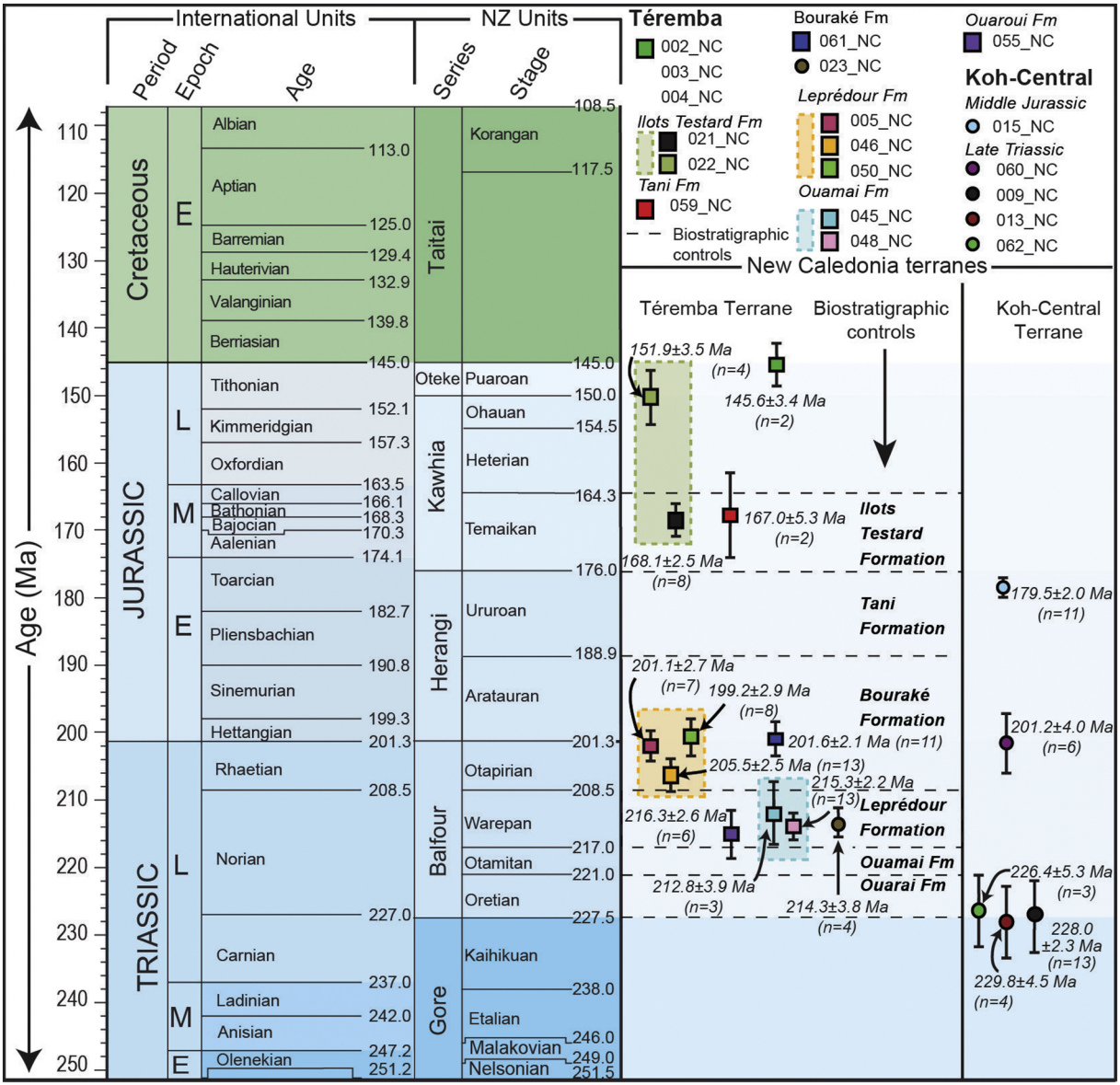
International Units
NZ Units
Period
Epoch
Age
Series
Stage
Age (Ma)
Cretaceous
JURASSIC
TRIASSIC
E
L
M
E
L
M
E
Albian
Aptian
Barremian
Hauterivian
Valanginian
Berriasian
Tithonian
Kimmeridgian
Oxfordian
Callovian
Bathonian
Bajocian
Aalenian
Toarcian
Pliensbachian
Sinemurian
Hettangian
Rhaetian
Norian
Carnian
Ladinian
Anisian
Olenekian
113.0
125.0
129.4
132.9
139.8
145.0
152.1
157.3
163.5
166.1
168.3
170.3
174.1
182.7
190.8
199.3
201.3
208.5
227.0
237.0
242.0
247.2
251.2
Taitai
Oteke
Kawhia
Herangi
Balfour
Gore
Korangan
Puaroan
Ohauan
Heterian
Temaikan
Ururoan
Aratauran
Otapirian
Warepan
Otamitan
Oretian
Kaihikuan
Etalian
Malakovian
Nelsonian
108.5
117.5
145.0
150.0
154.5
164.3
176.0
188.9
201.3
208.5
217.0
221.0
227.5
238.0
246.0
249.0
251.5
110
120
130
140
150
160
170
180
190
200
210
220
230
240
250
Téremba
002_NC
003_NC
004_NC
Ilots Testard Fm
021_NC
022_NC
Tani Fm
059_NC
Biostratigraphic controls
Bouraké Fm
061_NC
023_NC
Leprédour Fm
005_NC
046_NC
050_NC
Ouamai Fm
045_NC
048_NC
Ouaroui Fm
055_NC
Koh-Central
Middle Jurassic
015_NC
Late Triassic
060_NC
009_NC
013_NC
062_NC
New Caledonia terranes
Téremba Terrane
Biostratigraphic controls
Koh-Central Terrane
151.9±3.5 Ma (n=4)
145.6±3.4 Ma (n=2)
167.0±5.3 Ma (n=2)
168.1±2.5 Ma (n=8)
Ilots Testard Formation
Tani Formation
179.5±2.0 Ma (n=11)
201.1±2.7 Ma (n=7)
199.2±2.9 Ma (n=8)
201.6±2.1 Ma (n=11)
205.5±2.5 Ma (n=13)
Bouraké Formation
201.2±4.0 Ma (n=6)
215.3±2.2 Ma (n=13)
216.3±2.6 Ma (n=6)
212.8±3.9 Ma (n=3)
214.3±3.8 Ma (n=4)
Leprédour Formation
Ouamai Fm
Ouarai Fm
226.4±5.3 Ma (n=3)
228.0 ±2.3 Ma (n=13)
229.8±4.5 Ma (n=4)

Figure 5

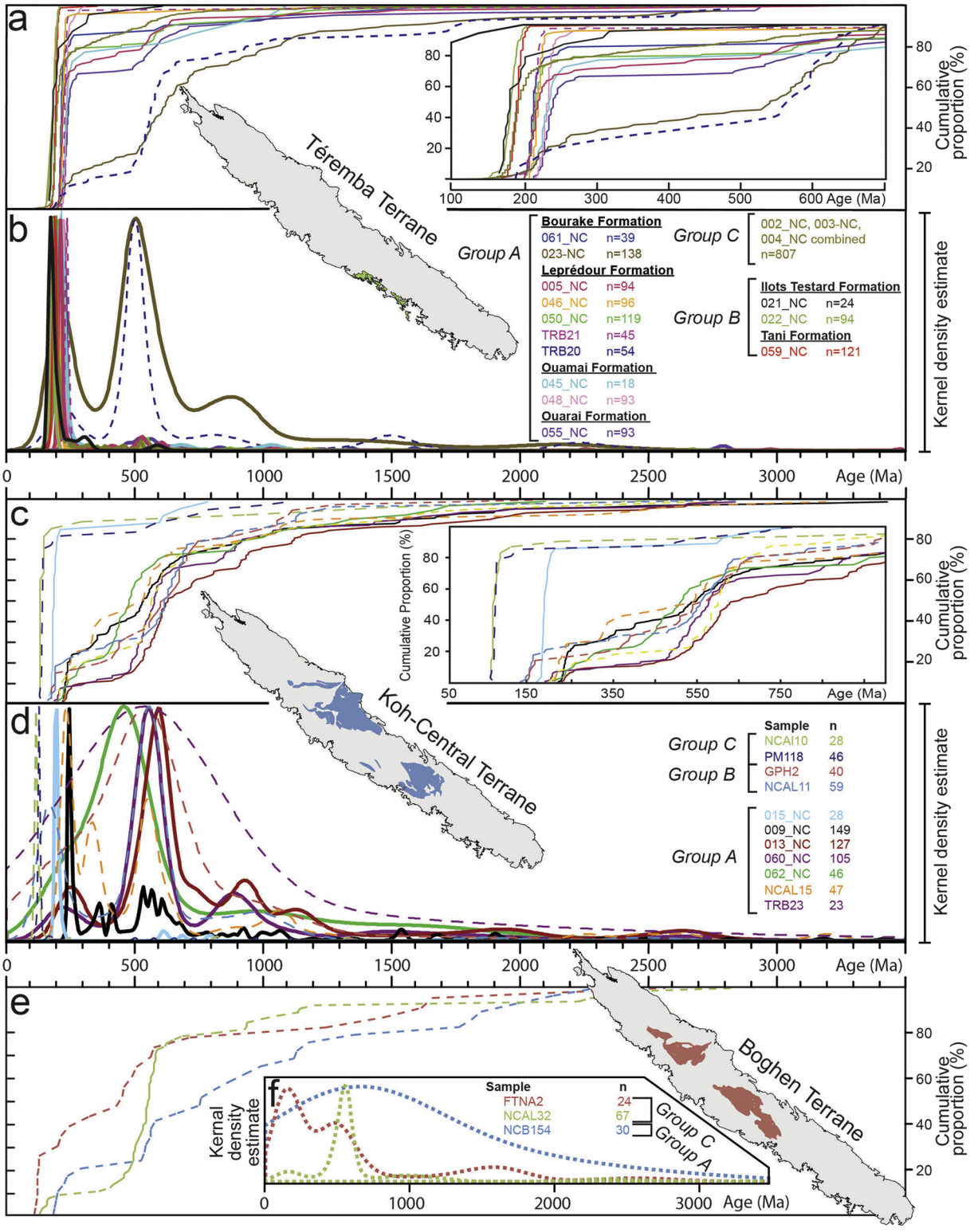
a
Cumulative proportion (%)
Térema Terrane
Group A
b
Bourake Formation
061_NC n=39
023-NC n=138
Leprédour Formation
005_NC n=94
046_NC n=96
050_NC n=119
TRB21 n=45
TRB20 n=54
Ouamai Formation
045_NC n=18
048_NC n=93
Ouarai Formation
055_NC n=93
Group C
002_NC, 003-NC, 004_NC combined n=807
Group B
Ilots Testard Formation
021_NC n=24
022_NC n=94
Tani Formation
059_NC n=121
Kernel density estimate
Age (Ma)
c
Cumulative Proportion (%)
Koh-Central Terrane
d
Sample n
Group C
Group B
NCAI10 28
PM118 46
GPH2 40
NCAL11 59
Group A
015_NC 28
009_NC 149
013_NC 127
060_NC 105
062_NC 46
NCAL15 47
TRB23 23
e
Boghen Terrane
f
Kernal density estimate
Sample n
FTNA2 24
NCAL32 67
NCB154 30
Group C
Group A

Figure 6

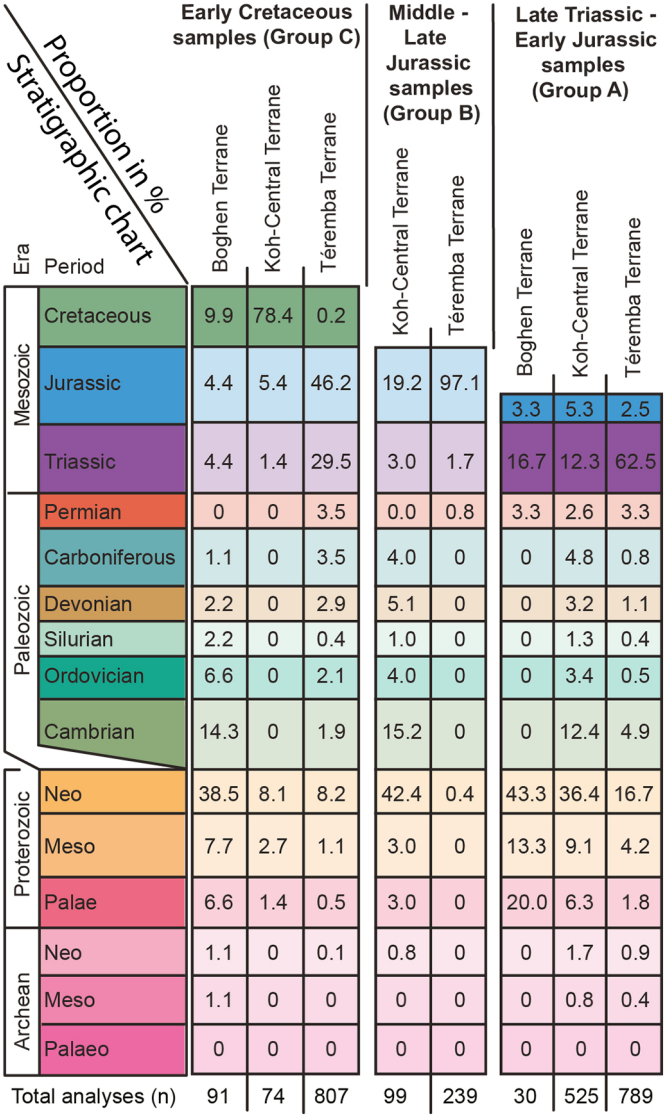
Proportion in %
Stratigraphic chart
Era
Period
Early Cretaceous samples (Group C)
Middle - Late Jurassic samples (Group B)
Late Triassic - Early Jurassic samples (Group A)
Boghen Terrane
Koh-Central Terrane
Téremba Terrane
Koh-Central Terrane
Téremba Terrane
Boghen Terrane
Koh-Central Terrane
Téremba Terrane
Mesozoic
Cretaceous 9.9 78.4 0.2
Jurassic 4.4 5.4 46.2 19.2 97.1 3.3 5.3 2.5
Triassic 4.4 1.4 29.5 3.0 1.7 16.7 12.3 62.5
Paleozoic
Permian 0 0 3.5 0.0 0.8 3.3 2.6 3.3
Carboniferous 1.1 0 3.5 4.0 0 0 4.8 0.8
Devonian 2.2 0 2.9 5.1 0 0 3.2 1.1
Silurian 2.2 0 0.4 1.0 0 0 1.3 0.4
Ordovician 6.6 0 2.1 4.0 0 0 3.4 0.5
Cambrian 14.3 0 1.9 15.2 0 0 12.4 4.9
Proterozoic
Neo 38.5 8.1 8.2 42.4 0.4 43.3 36.4 16.7
Meso 7.7 2.7 1.1 3.0 0 13.3 9.1 4.2
Palae 6.6 1.4 0.5 3.0 0 20.0 6.3 1.8
Archean
Neo 1.1 0 0.1 0.8 0 0 1.7 0.9
Meso 1.1 0 0 0 0 0 0.8 0.4
Palaeo 0 0 0 0 0 0 0 0
Total analyses (n) 91 74 807 99 239 30 525 789

Figure 7

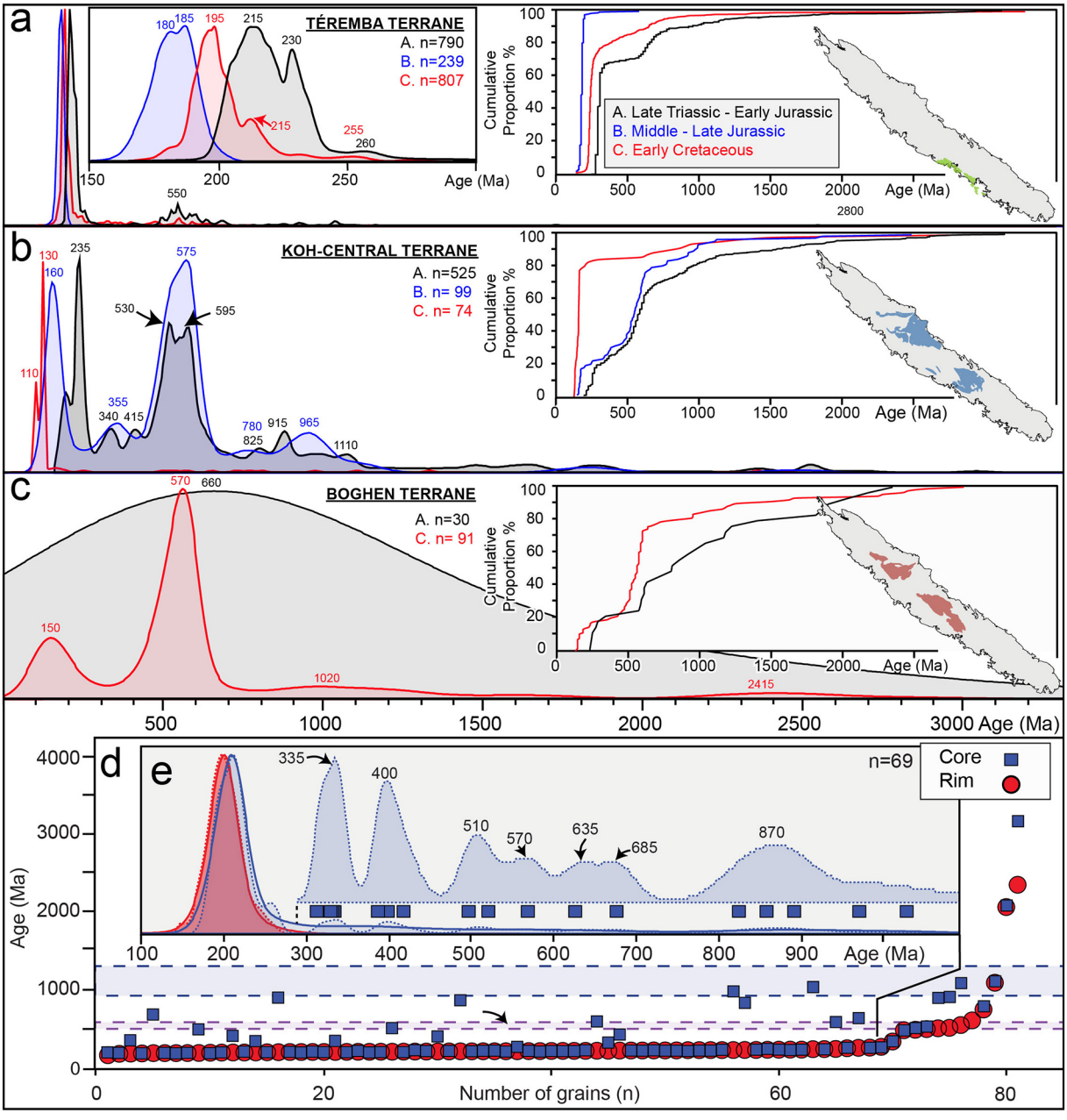
a
TÉREMBA TERRANE
A. n=790
B. n=239
C. n=807
180
185
195
215
230
215
255
260
150
200
250
Age (Ma)
550
Cumulative Proportion %
A. Late Triassic - Early Jurassic
B. Middle - Late Jurassic
C. Early Cretaceous
0
500
1000
1500
2000
Age (Ma)
2800
b
KOH-CENTRAL TERRANE
A. n=525
B. n= 99
C. n= 74
130
160
235
575
530
595
110
355
340
415
780
825
915
965
1110
c
BOGHEN TERRANE
A. n=30
C. n= 91
570
660
150
1020
2415
500
1000
1500
2000
2500
3000 Age (Ma)
d
e
n=69
Core
Rim
335
400
510
570
635
685
870
Age (Ma)
4000
3000
2000
1000
0
Number of grains (n)
20
60
80

Figure 8

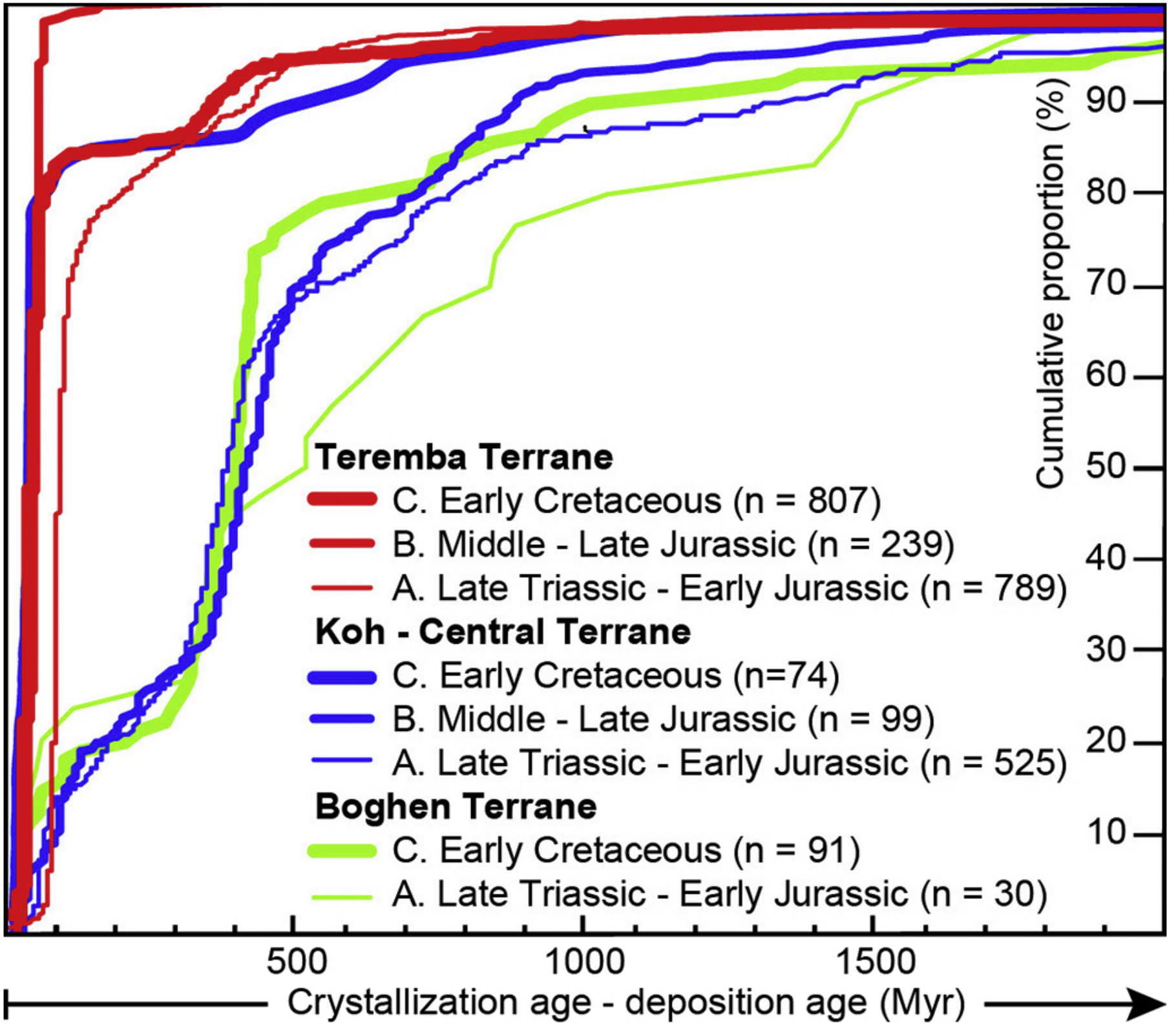
Teremba Terrane
C. Early Cretaceous (n = 807)
B. Middle - Late Jurassic (n = 239)
A. Late Triassic - Early Jurassic (n = 789)
Koh - Central Terrane
C. Early Cretaceous (n=74)
B. Middle - Late Jurassic (n = 99)
A. Late Triassic - Early Jurassic (n = 525)
Boghen Terrane
C. Early Cretaceous (n = 91)
A. Late Triassic - Early Jurassic (n = 30)
Cumulative proportion (%)
90
80
70
60
50
40
30
20
10
500
1000
1500
Crystallization age - deposition age (Myr)

Figure 9

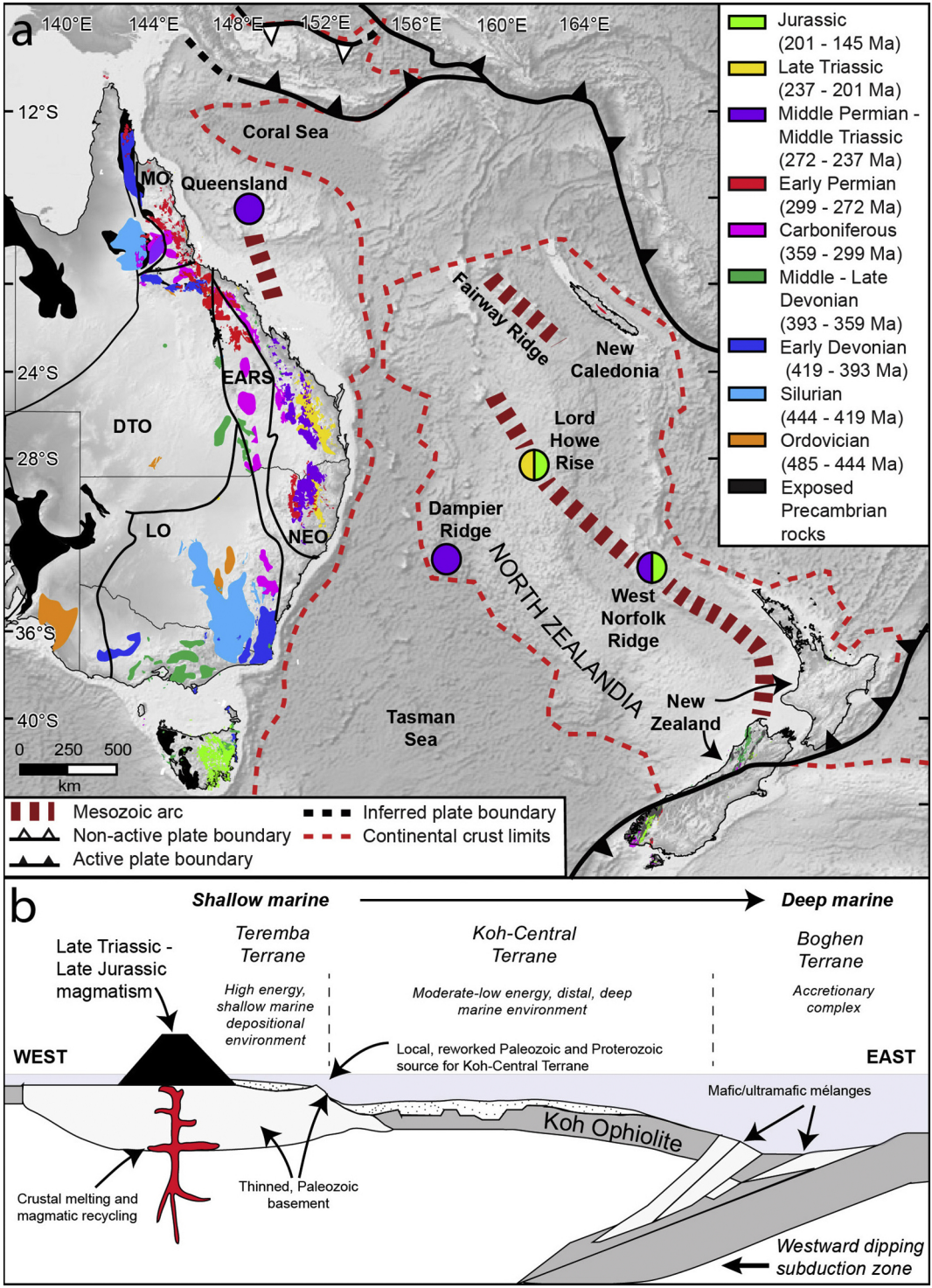
a
140°E
144°E
148°E
152°E
156°E
160°E
164°E
12°S
24°S
28°S
36°S
40°S
Coral Sea
Queensland
MO
EARS
DTO
LO
NEO
Fairway Ridge
New Caledonia
Lord Howe Rise
Dampier Ridge
NORTH ZEALANDIA
West Norfolk Ridge
New Zealand
Tasman Sea
0 250 500
km
Jurassic (201 - 145 Ma)
Late Triassic (237 - 201 Ma)
Middle Permian - Middle Triassic (272 - 237 Ma)
Early Permian (299 - 272 Ma)
Carboniferous (359 - 299 Ma)
Middle - Late Devonian (393 - 359 Ma)
Early Devonian (419 - 393 Ma)
Silurian (444 - 419 Ma)
Ordovician (485 - 444 Ma)
Exposed Precambrian rocks
Mesozoic arc
Non-active plate boundary
Active plate boundary
Inferred plate boundary
Continental crust limits
b
Shallow marine
Deep marine
Late Triassic - Late Jurassic magmatism
Teremba Terrane
High energy, shallow marine depositional environment
Koh-Central Terrane
Moderate-low energy, distal, deep marine environment
Boghen Terrane
Accretionary complex
WEST
EAST
Local, reworked Paleozoic and Proterozoic source for Koh-Central Terrane
Mafic/ultramafic mélanges
Koh Ophiolite
Crustal melting and magmatic recycling
Thinned, Paleozoic basement
Westward dipping subduction zone

Figure 10